Acoustic Scattering by Three-Dimensional Stators and Rotors Using the SOURCE3D Code

Volume 1: Analysis and Results

Harold D. Meyer
United Technologies Corporation, Windsor Locks, Connecticut

National Aeronautics and
Space Administration

Glenn Research Center

March 1999

Acknowledgments

TABLE OF CONTENTS

SUMMARY

This report presents a study of rotor and stator scattering using the SOURCE3D Rotor Wake/Stator Interaction Code. SOURCE3D is a quasi-three-dimensional computer program that uses three-dimensional acoustics and two-dimensional cascade load response theory to calculate rotor and stator modal reflection and transmission (scattering) coefficients. SOURCE3D is at the core of the TFaNS (Theoretical Fan Noise Design/Prediction System), developed for NASA, which provides complete fully coupled (inlet, rotor, stator, exit) noise solutions for turbofan engines.

The reason for studying scattering is that we must first understand the behavior of the individual scattering coefficients provided by SOURCE3D, before eventually understanding the more complicated predictions from TFaNS. As a first step toward understanding these coefficients, we have derived a large number of scattering curves for vane and blade rows and studied them for general trends. The curves are plots of output wave power divided by input wave power (in dB units) versus vane/blade ratio. This is a format that is suited both for physical as well as design study. A small sampling of these plots is provided here. All of the plots are provided in a separate volume. To assist in understanding the plots, formulas have been derived for special vane/blade ratios for which wavefronts are either parallel or normal to rotor or stator chords.

Work in this report was coordinated with concurrent work by D. B. Hanson who used two-dimensional analysis to derive parallel curves. In addition to allowing comparison between two- and three-dimensional based results, coordination with the two-dimensional case also allowed verification of the three-dimensional method. For the three-dimensional case, it was found that, for the most part, there was strong transmission and weak reflection over most of the vane/blade ratio range for the stator. Also, modes transmitted into themselves over large portions of the vane/blade ratio range. For the rotor, there was little transmission loss and, in a wide range of cases, modes transmitted into themselves or into themselves and nearby radial modes. The above stator and rotor trends were different from those for two-dimensions. Additionally, it was seen for rotor curves that scattered wave energy could sometimes be greater than input wave energy.

CHAPTER 1

INTRODUCTION

The TFaNS (Theoretical Fan Noise Design/Prediction System, Ref. 1) provides a methodology for turbofan harmonic noise prediction. Developed by Pratt and Whitney under contract to NASA Lewis, it seeks to obtain higher accuracy than previous three-dimensional codes by including all the acoustic elements of an engine – inlet, rotor, stator, exit (Fig.1.1) – in its formulation. In TFaNS, as in other codes, rotor wakes impinge on the stator, generating unsteady vane loads that produce noise. However, reflections from the inlet, rotor, and exit – missing from earlier approaches – are also included to provide additional sound contributions that should be present. The geometry is that of a three-dimensional annulus (Fig 1.2).

The fundamental behavior of TFaNS is governed by the rotor and stator scattering (reflection and transmission) coefficients. Because they are so central to TFaNS and because the output of TFaNS is so complex, we must first gain an understanding of them before expecting to understand the more general output of TFaNS, which comes from numerous modes reflecting back and forth and scattering into the same and other modes. Therefore, the object of the present work is to study the behavior of the reflection and transmission coefficients for the rotor and stator.

In TFaNS, scattering coefficients are defined in terms of duct eigenmodes and are determined for each of the engine elements in isolation. Also, source vector coefficients representing the interaction of the rotor wake with the stator are generated. Using this information, the acoustic elements are coupled by means of a matrix equation

$$A = SA + B,\qquad(1.1)$$

that matches acoustic input and output at the interface planes shown in Fig. 1.1. In Eq. (1.1), A is the state vector, which represents the modal amplitudes of the waves generated by the system. This vector has elements A^1, A^2, A^3 at the three interface planes. The quantity B is the source vector, made up of source vector coefficients; it has elements B^1, B^2, B^3 at the three interfaces. The parameter S is the scattering matrix, consisting of all the scattering coefficients. Solving Eq. (1.1) gives the state vector

$$A = (I - S)^{-1} B,\qquad(1.2)$$

which is used to calculate whatever output information is required. This process is described in further detail in Refs. 2 and 3.

The scattering coefficients, as well as the source vector coefficients, are calculated in TFaNS using the SOURCE3D Rotor Wake/Stator Interaction Code (Ref. 4) which is at the heart of TFaNS. It was developed at Hamilton Standard under NASA's Large Engine Technology Contract. It is SOURCE3D that has been used to generate the scattering curves central to this

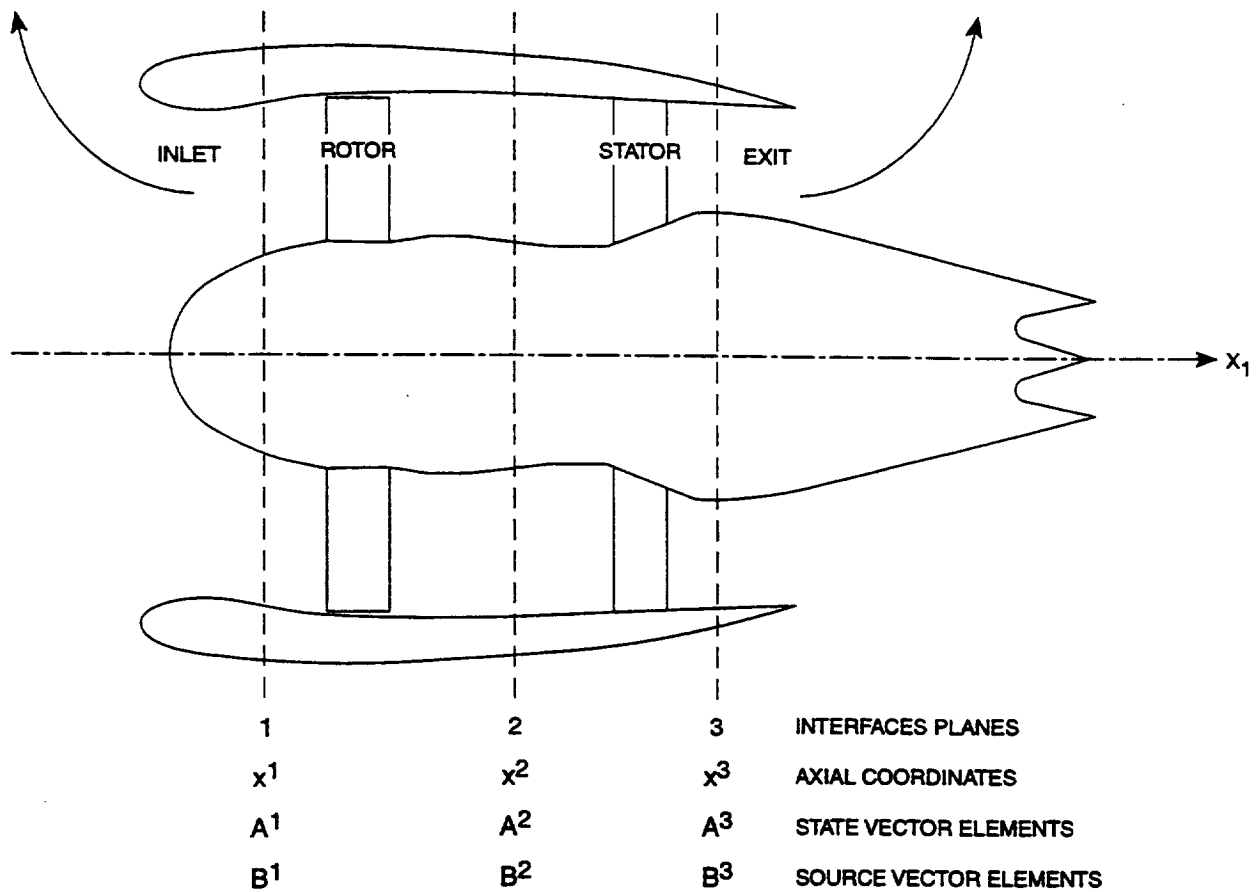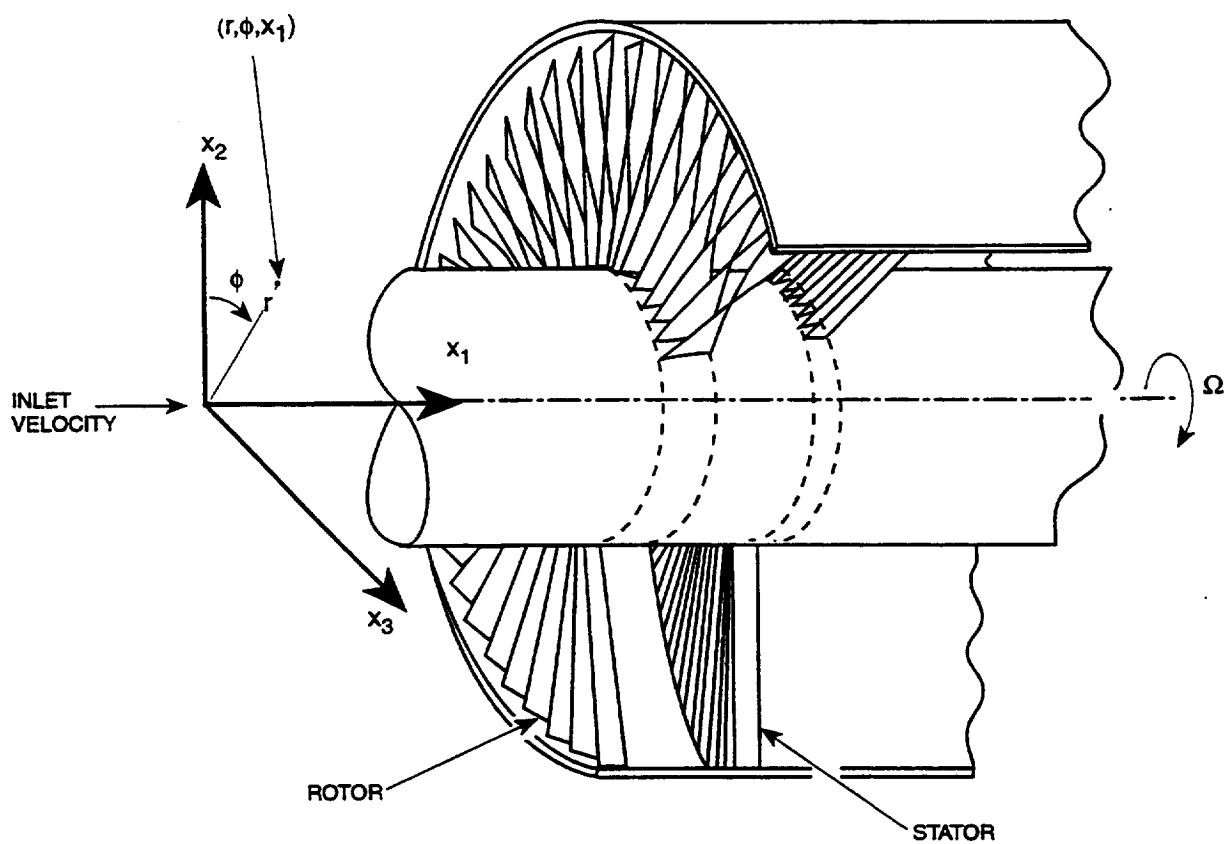|			INTERFACES PLANES
1	2	3	
x^1	x^2	x^3	AXIAL COORDINATES
A^1	A^2	A^3	STATE VECTOR ELEMENTS
B^1	B^2	B^3	SOURCE VECTOR ELEMENTS

FIGURE 1.1 TURBOFAN ACOUSTIC ELEMENTS

FIGURE 1.2 THREE-DIMENSIONAL TURBOFAN GEOMETRY

report.

SOURCE3D extends the ideas used by its predecessor, the V072 Rotor Wake/Stator Interaction Code (Ref. 5), to treat scattering in an annular duct by applying a combined three-dimensional/two-dimensional approach. In SOURCE3D, three-dimensional acoustic input waves impinge on stator vanes or rotor blades producing unsteady loads, which are calculated using two-dimensional strip theory. These loads are coupled to three-dimensional duct modes by means of the normal mode expansion of the three-dimensional Green's function for acoustic waves or by means of a variant of S. N. Smith's theory (Ref.6) for vorticity waves, which were not in V072. The output waves in both cases are three-dimensional. SOURCE3D provides rotor elements and includes swirl in the region between the rotor and stator, both of which also were absent from V072. It also adds actuator disks for flow turning and combines these with the rotor and stator elements to provide combined rotor/actuator disk and stator/actuator disk elements. With all these additions, SOURCE3D permits both frequency scattering and mode trapping, which are necessary in obtaining more accurate noise predictions. Background axial flow in SOURCE3D is uniform in each element region, while swirl is of solid body type. The unsteady flow is subsonic and isentropic.

Work here was coordinated with parallel work for the two-dimensional approach by D. B. Hanson (Ref. 2). Both studies use the same test cases and a similar format for presenting results. Studying the two has provided a baseline from which to see the difference a three-dimensional approach makes, in addition to just splitting circumferential modes into radial mode components. Many three-dimensional results were similar to those for two dimensions; however, there are exceptions that will be seen later.

In material that follows, we start with a "background and preliminaries" section which briefly discusses geometry and a definition of standard waves and scattering coefficients. We also discuss the format for the curves that present our results as well as discussing cut-on range and special points on the curves. In the next chapter, the main results of the report are described for two test cases – one at a mid speed rotor rotational speed and the second at a high speed rotational speed. The results are based on a very large collection of scattering curves. Only a small sampling of these plots is shown here. All of the plots are provided in a separate volume (Ref. 7). Much of the background for work in this report appears in more detail in other papers. Therefore the reader may wish to consult the references cited in particular sections when additional details are desired.

CHAPTER 2

BACKGROUND AND PRELIMINARIES

2.1 Standard Waves and Scattering Coefficients

In SOURCE3D, the geometry is that of the annular duct shown in Fig. 1.2. As seen in the figure, the coordinate system is cylinder polar with the polar axis x_1 oriented along the duct centerline. The coordinate x_1 increases in the direction of air flow and may have its origin at different locations depending upon the situation. The rotor rotates in the direction of positive polar angle ϕ with fan rotational speed Ω. The duct has outer radius r_D and inner radius r_H. Fig. 2.1 shows the intersection of the stator vanes and rotor blades with a cylindrical surface of radius r. The stator has V equally spaced identical vanes with spacing $2\pi r / V$. The same is true for the rotor, only spacing is $2\pi r / B$. The vane stagger angle is α_S and its local semi-chord is b. For the blades, the rotor stagger angle is $-\alpha_R$ and the local semi-chord is b_R. The rotor stagger angle is defined in this manner to be consistent with the definition in Ref. 4.

SOURCE3D treats three types of waves – upstream-going pressure waves, downstream-going pressure waves, and one type of downstream-going vorticity wave. In this report, we will only study scattering coefficients for the pressure waves, so vorticity waves will not be of treated. The pressure waves are described in terms of standard modes. This means that pressure p_W^P is given by the expression

$$p_W^P(x_1, r, \phi, t) = p_\infty \sum_{s=-\infty}^{\infty} \sum_{k=-\infty}^{\infty} \sum_{n=1}^{\infty} A_{Wskn}^P \Psi_{mn}(r) e^{i[m\phi - \gamma_{Wskn}^P(x_1 - x^P) - sB\Omega t]}. \tag{2.1}$$

Here, s is the blade passing frequency (BPF) harmonic index; k, the vane passing frequency harmonic index; n, the duct radial mode index; m, the circumferential mode order, given by $m = sB - kV$; and t is time. The function $\Psi_{mn}(r)$ is the standard duction radial mode, given in terms of Bessel functions. These functions have eigenvalues κ_{mn}. Radial mode indices here start at $n = 1$ to stay consistent with the convention in V072. Standard practice in many other places is to use an index $\mu = n - 1$ so that counting starts at 0. Note that, for the two-dimensional case in Ref. 2, n, rather than s, has been used for the BPF harmonic index. However, k is still the vane passing frequency harmonic index. Also, $m = nB - kV$. There is no radial mode index because there are no radial modes in two dimensions.

The standard waves have their origins at the axial interface locations x^P, where $P = 1, 2, 3$ (see Fig.1.1). Also, x^P may represent the axial locations x^S where the stator leading edge meets the hub or x^R where the rotor leading edge meets the hub. Generally, for derivations here, coordinate systems have been defined, for convenience, so that either $x^S = 0$ or $x^R = 0$. In
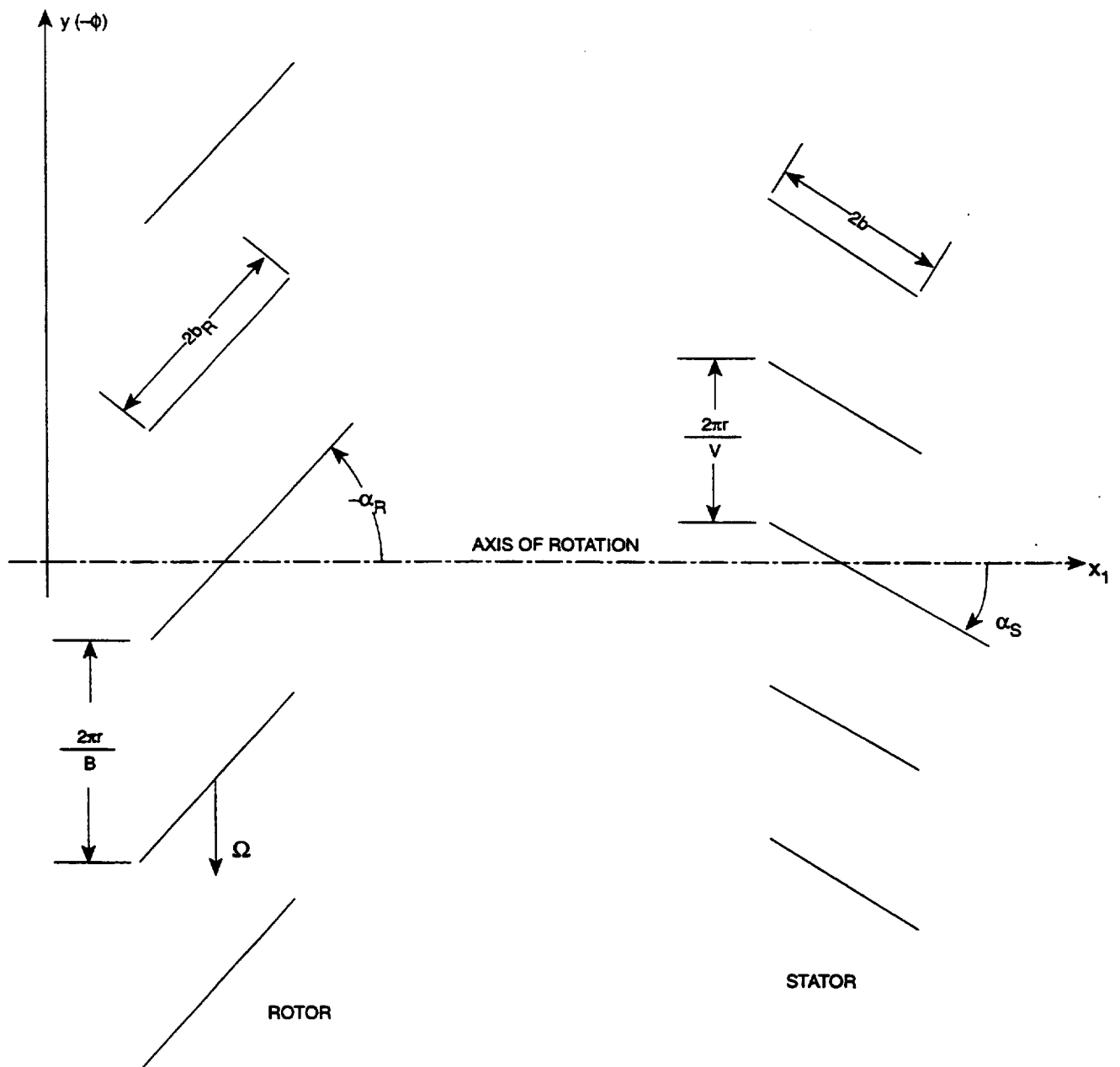
FIGURE 2.1 ROTOR/STATOR GEOMETRY

Eq. (2.1), the subscripts W indicate wave type: for $W = 1$, the wave is upstream-going; when $W = 2$, it is downstream-going. The parameters A^P_{Wskn} are state vector coefficients and represent pressure modal amplitudes. They are normalized by the far-field pressure p_∞ and will be used below to define our scattering coefficients. They make up the elements used to specify the state vectors A discussed in Chapter 1. The quantities γ^P_{Wskn} are the axial wavenumbers, which are given by

$$\gamma^P_{Wskn} = \frac{1}{\beta^2 r_D}[m(sBM_T - mM_s) \pm k^P_{Wskn}],\qquad(2.2)$$

where the upper sign (+) is for upstream-going waves ($W = 1$), and the lower sign (-) is for downstream-going waves ($W = 2$). Further, M is the axial flow Mach number; M_T, the rotor blade tip rotational Mach number; M_s, the swirl rotational Mach number at the rotor tip (not to be confused with M_S used in Ref. 4 for the axial flow Mach number in the stator region); $\beta = \sqrt{1 - M^2}$; and

$$k^P_{Wskn} = \sqrt{(sBM_T - mM_s)^2 - \beta^2 \kappa^2_{mn}}.\qquad(2.3)$$

Values of the Mach numbers and β in Eq. (2.3) are those for the regions associated with P.

As discussed in Refs. 3 and 4, upstream- and downstream-going pressure waves will each scatter into both upstream- and downstream-going pressure waves.* When viewed from a stationary coordinate system, input waves with indices s_i, k_i, n_i will be scattered by the stator into waves with index s_i, but not necessarily into waves with indices k_i and n_i. These same waves will be scattered by the rotor into waves with index k_i, but not necessarily with indices s_i and n_i. We represent this process schematically by

Stator: $s_i, k_i, n_i \rightarrow s_i, k, n$,
Rotor: $s_i, k_i, n_i \rightarrow s, k_i, n$.

For such interactions, we define the scattering coefficients, $S^{PP_i}_{WW_i skn; s_i k_i n_i}$, as the ratios, $A^P_{Wskn} / A^{P_i}_{W_i s_i k_i n_i}$, of output to input wave state vectors, where P_i and W_i are values of P and W for input waves. This ratio is equivalent to the value of the output wave mode amplitude produced by a unit modal input wave, i.e. one having $A^{P_i}_{W_i s_i k_i n_i} = 1$. Schematically, we represent the scattering process by

$$A^P_{Wskn} \leftarrow S^{PP_i}_{WW_i skn; s_i k_i n_i} A^{P_i}_{W_i s_i k_i n_i}.$$

---

* They also scatter into downstream-going vorticity waves. This is included in the analysis, but vorticity wave results are not presented here.

2.2 Plot Format and Special Points

For this study, we have presented our results in the form of plots of power ratios versus vane/blade (*V/B*) ratio (e.g. the plots in Chapter 3). The power ratios are for either reflection or transmission and are defined as the dB value of the quotient of the output wave power divided by the input wave power. This quantity is given in terms of scattering coefficient values as specified by Eq. (A.26) of Appendix A, where power relations are derived. The present format, where *V/B* varies, was chosen because it corresponds to the approach used in design work. It is different from the format sometimes also used (see, for instance, S. N. Smith's investigation in Ref. 6), where reduced frequency is held constant.

In the design approach, often the solidities of the rotor and stator blade rows are kept fixed because of aerodynamic requirements. The same is true for flow angles and Mach numbers which are fixed by pressure ratio and tip speed requirements. Thus, in runs here, these parameters have been kept fixed and only *V/B* ratio has been varied, which is equivalent to varying reduced frequency. To see this equivalence, note that the reduced frequency, ω_S, for the stator, is given by

$$\omega_S = \frac{\omega b}{U_{rS}} = \frac{sB\Omega b}{M_{rS}c_0} = \frac{2\pi(sB\Omega r_D / c_0)}{VM_{rS}}\left(\frac{bV}{2\pi r_D}\right)$$
$$= 2\pi\left(\frac{sB}{V}\right)\frac{M_T}{M_{rS}}\sigma_S,$$

(2.4)

where ω is radian frequency; c_0 is the speed of sound; U_{rS} is fluid velocity relative to the stator; M_{rS} is the corresponding Mach number; and $\sigma_S = bV / 2\pi r_D$ is the stator solidity. Because M_T, M_{rS}, and σ_S are fixed for the runs, reduced frequency ω_S varies when *V/B* varies. The same is true for the rotor, because its reduced frequency, ω_R, is given by

$$\omega_R = \frac{\omega b_R}{U_{rR}} = \frac{kV\Omega b_R}{M_{rR}c_0} = \frac{2\pi(kV\Omega r_D / c_0)}{BM_{rR}}\left(\frac{b_R B}{2\pi r_D}\right)$$
$$= 2\pi\left(\frac{kV}{B}\right)\frac{M_T}{M_{rR}}\sigma_R,$$

(2.5)

where U_{rR}, M_{rR}, and σ_R are the analogs of the stator quantities above.

In studying the curves generated for this report, the main thrust will be to investigate the general trends. However, it will also be useful to consider a number of special vane/blade ratio points that might also provide understanding in interpreting the results. The first of these points is actually a range of points. It is that set of *V/B* values, for a given M_T, where both the input and output waves for a particular scattering coefficient are cut on (i.e., where both these waves are propagating waves for the particular modal indices involved). Outside this cut-on range, waves are said to be cut-off waves. See Ref. 5 for a discussion of cut on and cut off. To obtain non-zero scattering coefficients, both the input and output waves must be cut on. A formula giving

- 8 -

the cut-on range in terms of V/B and M_T is derived in Appendix B and is shown graphically in Fig. 2.2. Such information is useful in that it allows us to see where non-zero values for a given scattering coefficient should start and end on our plots. Note that the boundary lines in Fig. 2.2 are sketched as straight (which is exactly true in two dimensions), although, as discussed in Appendix B, this is only an approximation for the three-dimensional situation. Also, note that the the boundary lines in Fig. 2.2 depend on radial mode index n. This is different from the two-dimensional case, where there are no radial modes.

A special value of V/B occurs when the normal distance between two stator vanes or rotor blades is half the length of the free space acoustic wavelength. The condition that occurs at this value is called "load divergence" and would be expected to produce large values of reflection or transmission coefficients. The formula specifying where this V/B is located is given in Appendix B. Note that the value of V/B for this case was dependent on radius r, as will also be the case for several other of our special points. Because these special conditions may occur at only one r for a given V/B, it is possible for the associated effects to be weak. Note, however, that for load divergence this observation may not hold – pressure loading could be sufficiently large, even if at just one radius, to produce unrealistically high power ratios. Also, note that, for load divergence, it was observed from computer runs that maximum blade loading generally occurred near the hub ($r = r_H$). Therefore, we have set $r = r_H$ in the formula for load divergence. For other special cases, below, where formulas are also dependent on r, we would expect, however, that the effects would be strongest for $r/r_D = 0.8$, which is roughly where maximum loading ordinarily occurs. Therefore, we have set $r/r_D = 0.8$ in the formulas for those cases. Note that, for the two-dimensional approach (Ref. 2), this radial consideration does not arise, because only r_D is used.

Power ratio values are also large near the condition called "duct resonance," which occasionally occurs at V/B ratios very close to cut on. These power ratios are overpredicted because of limitations in the original V072 model that carry over to SOURCE3D. When these large values occur, it is normally obvious to the user. As discussed in Ref. 4, this condition is caused by an inconsistency in the manner in which the unsteady blade loading and the acoustic modes are calculated. The three-dimensional mode coupling equation has a quantity k_{skn} in the denominator that goes to zero at cut off. In a fully consistent three-dimensional method, this limit would be offset by loading in the numerator that also approaches zero at cut off. However, because of the mixture of two-dimensional aerodynamic theory and three-dimensional duct acoustic theory, these cut-off conditions occur at different values of frequency (or RPM or V/B ratio). Hence, near three-dimensional cut off, the scattering results are not reliable. This difficulty has been somewhat reduced in the SOURCE3D code by using a "k_{skn}-patch," whereby, when a frequency very near to cut on is reached, k_{skn} is fixed at the value here and not allowed to decrease further in a band about cut on.

Another special case is "channel resonance." This condition occurs when standing waves, with distance between nodes the same as the chord, or channel, length, form between the vane or blade rows. Formulas predicting the V/B ratios for this phenomenon are derived and presented in Appendix B. Because the results are dependent on radius r, the formulas are evaluated at $r/r_D = 0.8$, as discussed above. Similar to the load divergence case, since pressure loading even at just
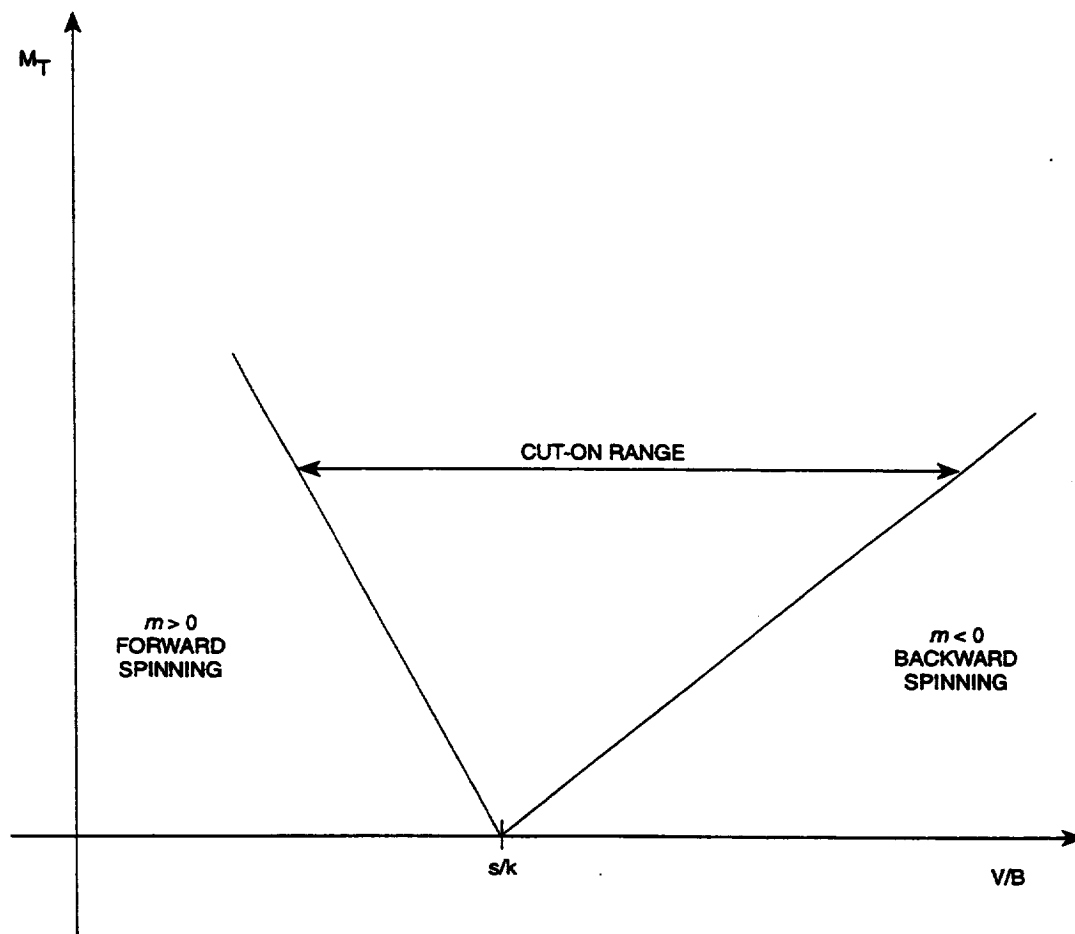
FIGURE 2.2 CUT ON RANGE FOR A GIVEN VALUE OF RADIAL MODE INDEX *n*

one r could be very large, we might expect the effect to be stronger than otherwise. However this does not occur, as will be seen later, when we inspect the curves.

Finally, there are three special values of V/B when wavefronts are either parallel or perpendicular to the airfoils. First, when they are parallel, we have the "broadside" case (see Figs. 2.3 and 2.4 for the stator and rotor) where significant reflection might be expected. Second, when input waves are perpendicular to the chord lines, we would expect waves to pass right through the vane or blade rows, so that reflection would be low and transmission high. This situation is called the "venetian blind" case and is shown in Fig. 2.5 for the stator. The third is a similar condition where input waves are not necessarily normal to the chords, but the reflected waves are. This is called the "modal" case, and, for it, we would expect that reflection coefficients would be smaller. Formulas for the above three cases are derived and displayed in Appendix B. It should be noted that only the value of V/B for the broadside case is independent of radius r. Hence, we might expect that this effect would be significant on the curves, but it is not. For the other cases, the values found for V/B depend on r, so r/r_D is set, as before, to 0.8 in the formulas for identifying modal points on the scattering curves.
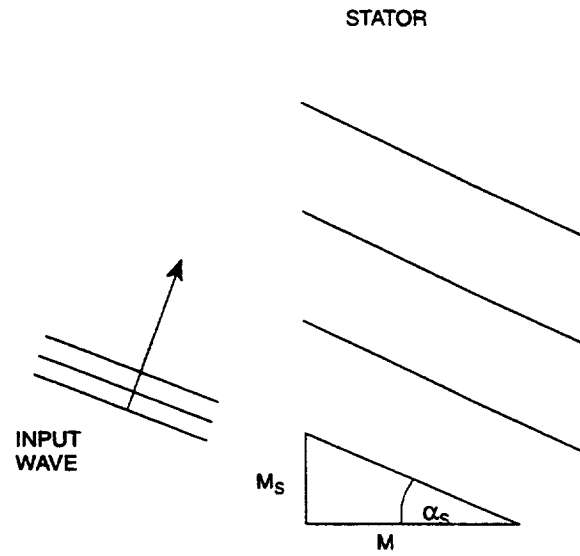
STATOR

INPUT
WAVE

M_S

α_S
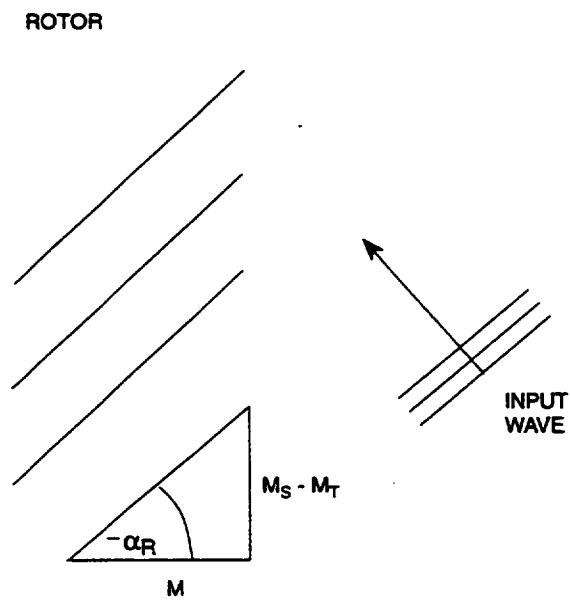
M

FIGURE 2.3 "BROADSIDE" CASE FOR STATOR

ROTOR

INPUT
WAVE

$M_S - M_T$

$-\alpha_R$

M

FIGURE 2.4 "BROADSIDE" CASE FOR ROTOR

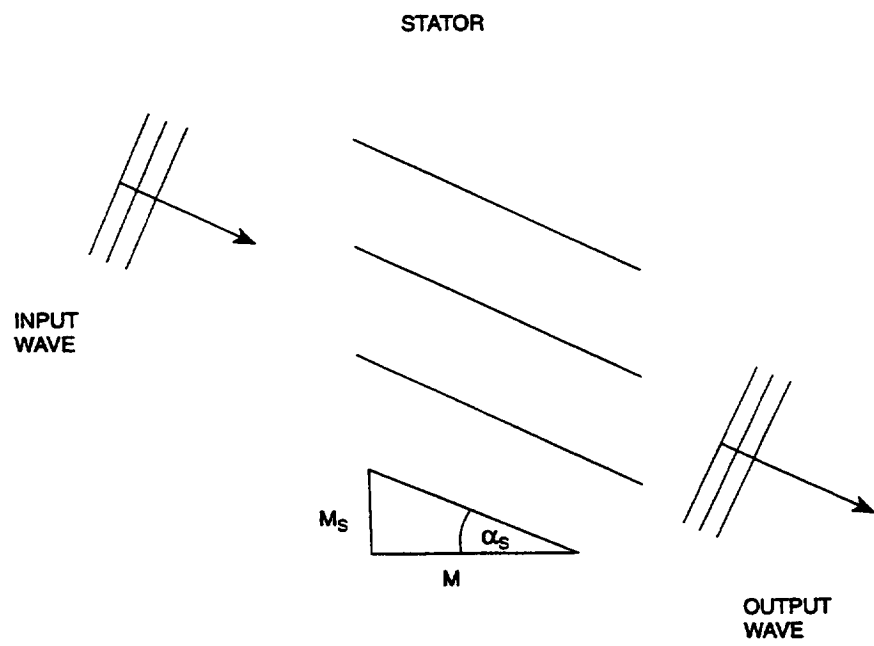STATOR

INPUT
WAVE

M_S

α_S

M

OUTPUT
WAVE

FIGURE 2.5 "VENETIAN BLIND" CASE FOR STATOR

CHAPTER 3

SCATTERING RESULTS

As mentioned previously, we have plotted dB values of (output wave power/input wave power) ratios versus vane/blade (V/B) ratio. A level of 0 dB is equivalent to unit reflection or transmission. We have swept out a V/B range of roughly 0.5 to 2.5, while keeping the solidities, σ_S and σ_R, of the stator and rotor constant. In studying the curves, we have looked at both the special points discussed in the previous chapter and at general trends. Work here was coordinated with a parallel two-dimensional study (Ref. 2), with both supported by the same NASA contract. Both studies used the same geometry and operating conditions, though the model was somewhat simpler in the two-dimensional case. For instance, the two-dimensional model uses only tip radius, while the three-dimensional one employs the entire span between hub and tip radial stations. Also, the three-dimensional investigation is based on radial and circumferential mode order, rather than just circumferential modes, as in the two-dimensional case.

Before beginning the actual test runs, the three-dimensional geometry was tested using a thin annulus. As expected, the SOURCE3D runs employing this model gave the same power ratios as given by D. B. Hanson's CUP2D runs.

The test cases for this report are based on the Pratt & Whitney 22 inch Advanced Ducted Propeller (ADP) model referred to as "Fan 1." It has 45 vanes and 18 blades; however, for computer runs, the vane number was varied while keeping stator and rotor solidities fixed. Flow was axial downstream into the rotor and then past the stator. Between rotor and stator, there was also solid body swirl. To establish operating conditions, rotor rotational speed Ω, inlet axial Mach number M, and pressure ratio were first set, then remaining conditions were calculated assuming two-dimensional isentropic flow (see Ref. 2). Two of the Pratt & Whitney cases, "mid speed" and "high speed," were studied. Operating conditions for the two cases are shown in Table 1, where p_∞ is far-field pressure and a_∞ is far-field speed of sound.

Scattering curves for the mid speed and high speed cases are presented, separately, in Ref. 7. There were a total of 648 plots. Because our main interest is the rotor/stator interaction, input waves for the plots all have their starting point between the two blade rows. In the plots, input waves for the stator and rotor have modal indices (s_i, k_i, n_i) ranging from (1,1,1) to (3,3,3). Output waves have indices (s, k, n) satisfying the scattering requirements discussed in Section 2.1 and fall in the same range. Note that output for all additional cut-on k's and n's was calculated in totals in the SOURCE3D runs, but was not included as curves on the plots.

Typical sets of stator and rotor plots for one particular choice of input wave, the (1,1,1) mode, are shown, respectively, in Figs. 3.1 and 3.2. Reflection curves appear at the top and transmission curves at the bottom. Each plot has curves for the three output radial modes, $n = 1$, 2, 3. The special points of Chapter 2 are also shown on the curves. These points and the

Stator Reflection-Mid Speed Case
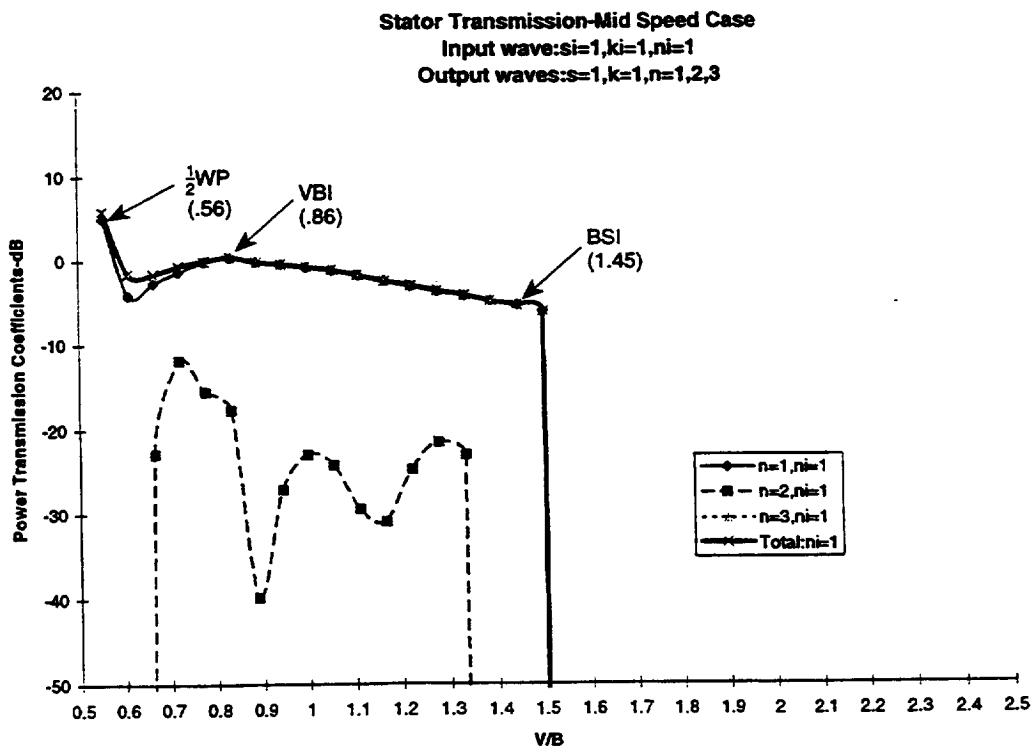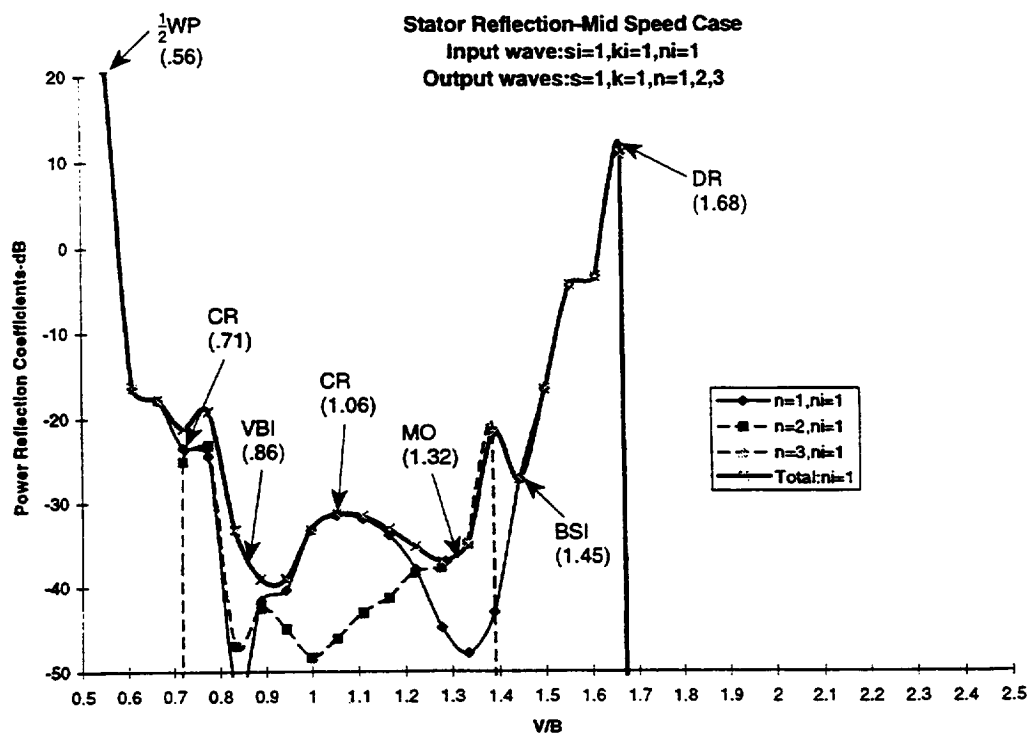Input wave:si=1,ki=1,ni=1
Output waves:s=1,k=1,n=1,2,3

Stator Transmission-Mid Speed Case
Input wave:si=1,ki=1,ni=1
Output waves:s=1,k=1,n=1,2,3

**FIGURE 3.1   STATOR SCATTERING – FUNDAMENTAL
(1,1,1) MODE INPUT FROM ROTOR SIDE**

Rotor Reflection–Mid Speed Case
Input wave:si=1,ki=1,ni=1
Output waves:s=1,k=1,n=1,2,3

Rotor Transmission–Mid Speed Case
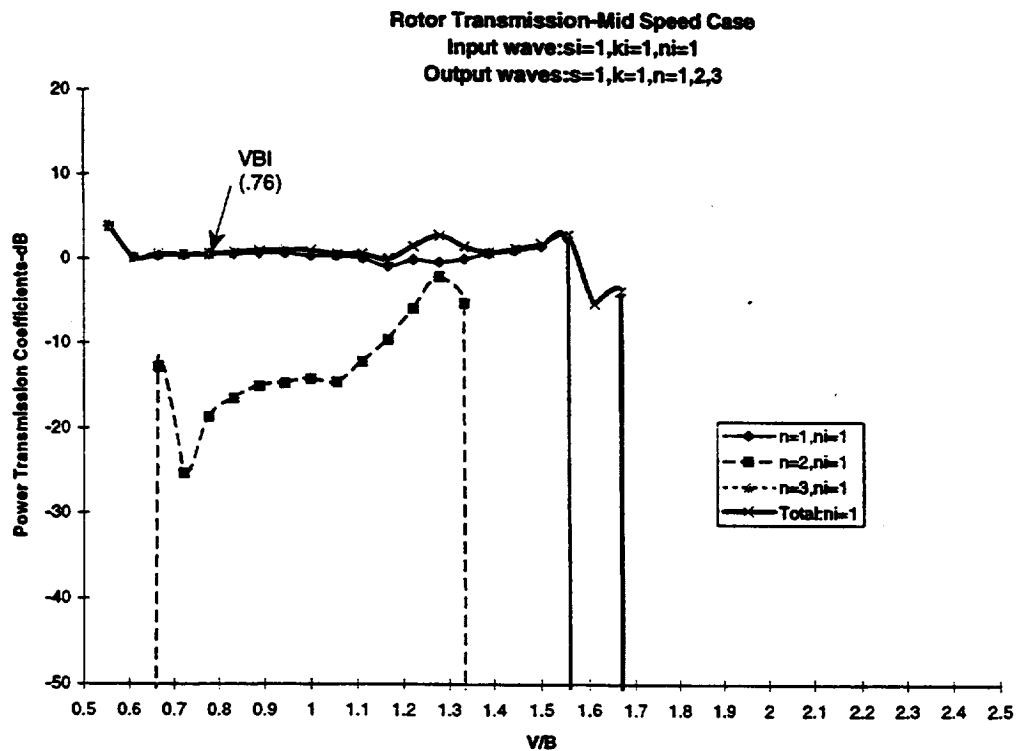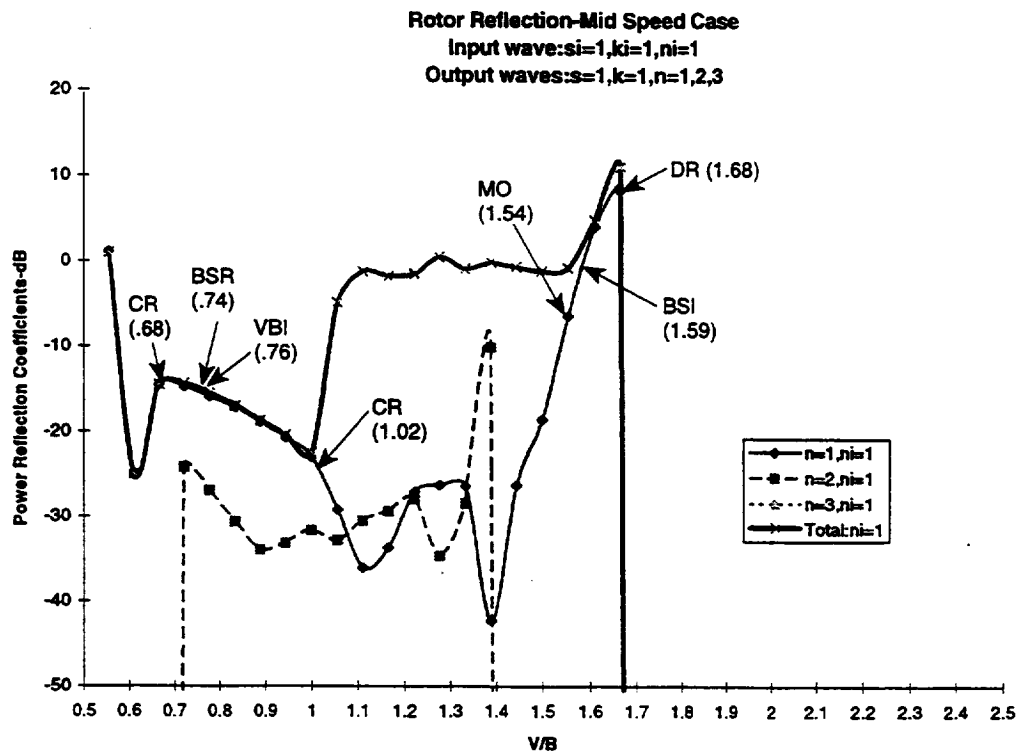Input wave:si=1,ki=1,ni=1
Output waves:s=1,k=1,n=1,2,3

FIGURE 3.2   ROTOR SCATTERING – FUNDAMENTAL (1,1,1)
MODE INPUT FROM STATOR SIDE

- 16 -

abbreviations, ½WP, CR, DR, VBI, MO, and BSI, used for them, will be discussed later. Associated with the input index (1,1,1) are two other sets of plots, which appear in Ref. 7, but which do not appear here. For the stator, there would be plots for the output indices ($s = 1$, $k = 2$, $n = 1,2,3$) and ($s = 1$, $k = 3$, $n = 1,2,3$). For the rotor, there would be plots for the output indices ($s = 2$, $k = 1$, $n = 1,2,3$) and ($s = 3$, $k = 1$, $n = 1,2,3$). In Ref. 7, this pattern carries over for each choice of input indices. . The types of plots shown in Figs. 3.1 and 3.2 are also given for input radial mode indices of $n_i = 2$ and 3 in Ref. 7.

It was mentioned above that output for additional cut-on k's and n's is calculated in the SOURCE3D runs, but has not been plotted. This information has, however, been included in obtaining the total power curves that appear in Figs. 3.1 and 3.2. For the stator, the total power curves give the sums of the power ratios for all of the cut-on output modes, either for reflection or transmission, for a given input wave. The setup for the rotor scattering curves is similar. However, the total power curves for the rotor include only contributions from those cut-on output modes whose harmonic indices fall between $s = -3$ and $s = 3$, because of the manner in which output was collected for the plots. Note that the same total power curve is carried over from plot to plot for all three plots associated with a given input wave (see, for instance, Figs. 3.5-3.7, that appear later). The total power curve represents the sum described above, not just the sum of those curves appearing on a particular figure.

Table 1. Operating Conditions

	Mid Speed	High Speed
Corrected RPM	7031	8750
Pressure Ratio	1.180	1.278
Axial Mach Nos.: Regions 1,2,3*	0.404, 0.350, 0.341	0.510, 0.404, 0.388
Swirl Mach Nos. (Tip): Regions 1,2,3*	0.000, 0.199, 0.000	0.000, 0.238, 0.000
Tip Rot'l. Mach Nos.: Regions 1,2,3*	0.614, 0.600, 0.597	0.772, 0.742, 0.738
Mean Pressure/ p_∞: Regions 1,2,3*	0.894, 1.055, 1.089	0.837, 1.099, 1.152
Total Pressure/Inlet Tot. Pres.: Regions 1,2,3*	1.000, 1.180, 1.180	1.000, 1.278, 1.278
Sound Speed/ a_∞: Regions 1,2,3*	0.984, 1.008, 1.012	0.975, 1.014, 1.020
Stator Solidity (Tip)	1.091	1.091
Rotor Solidity (Tip)	1.039	1.039
Stator Stagger Angle (Tip)	29.6°	30.5°
Rotor Stagger Angle (Tip)	48.8°	51.3°

* Region 1 = upstream of rotor; Region 2 = between rotor and stator; Region 3 = downstream of stator.

Let us focus on the curves in Figs. 3.1 to obtain an initial understanding of scattering coefficient behavior. Here we see that the (1,1,1) input wave scatters into the (1,1,1), (1,1,2), and (1,1,3) modes. (It also scatters into (1,2,1), (1,2,2), and (1,3,1) modes which are not shown here, but are shown on plots in Ref. 7.) As can be calculated from Eq. (B.1), using data from the computer run, the input wave cuts off at $V/B = 1.68$. This is seen in Fig. 3.1, where the total power curves for reflection and transmission drop off at their right-hand ends. With regard to individual output modes, observe that the (1,1,2) reflected wave cuts on at 0.70 and cuts off at 1.41, which can be seen in Fig. 3.1. As can be seen from the transmission curve for this mode, the cut-off limits for transmitted output waves are different. This occurs because the transmitted waves fall in Region 3, while the reflected ones fall in Region 2. Because the Mach numbers are different for the two regions, Eq. (B.1) gives different values.

Observe next the special V/B points displayed on Fig. 3.1. These were defined earlier in Section 2.2 and have been calculated using the formulas presented in Appendix B. On the curves, ½WP represents a half wave point; CR, a channel resonance point; DR, a duct resonance point; VBI, a venetian blind input wave point; MO, a modal scattered wave point; and BSI, a broadside input wave point. The V/B values where these conditions occur are shown in parentheses.

With regard to these points, first observe that the half wave points in Fig. 3.1, at V/B = 0.56, explain why the ordinate values there are so large. Half wave, or load divergence, points are points at which blade loading becomes large. Next note that channel resonance points at V/B = 1.06 ($q = 2$) and 0.71 ($q = 3$) in the reflection plot of Fig. 3.1, which are points where organ pipe type behavior could occur, did not show any particular pattern. The parameter q is the non-zero integer appearing in Eq. (B.6). One value was near a local maximum, the other near a local minumum, and other points, not shown here, were at neither. Channel resonance points showed no particular pattern, also, in the two-dimensional case. A duct resonance point occurs near cut off for the (1,1,1) input wave. This can be seen on the reflection plot of Fig. 3.1 at $V/B = 1.68$. This condition explains the high ordinate at this point. When duct resonance occurs here or elsewhere, it is usually obvious to the analyst that this condition has occurred, and the value should be disregarded. Recall that 0 dB indicates reflected power equal to input power. It has been found for two-dimensional stators (Ref. 2) that reflection coefficients do not exceed 0 dB. If this behavior carries over to three dimensions, then values above 0 dB should be ignored.

VBI type points, for the stator, occur when input wave fronts are normal to chord lines. These points are shown at $V/B = 0.86$ in Fig. 3.1, and, similar to the two-dimensional case, show a definite effect. Input waves transmit through the vane row with virtually no scattering, and there is very little reflection. Looking at occurrences here and on curves not shown, we see that transmission is high or at a peak and reflection is at or near dips in the plots. MO points are also shown on Fig. 3.1. For these points, which occur at $V/B = 1.32$, the wave fronts are also perpendicular to the vane chords; however, now, the waves traveling in this direction are output waves only. In this situation, the reflected waves are normal to the vane loading dipoles, so cannot couple to them. Thus, where they appear in our reflection curves, here and on others not shown, they generally, but not always, appear at dips. However, this condition does not appear as strong as for the two-dimensional case.
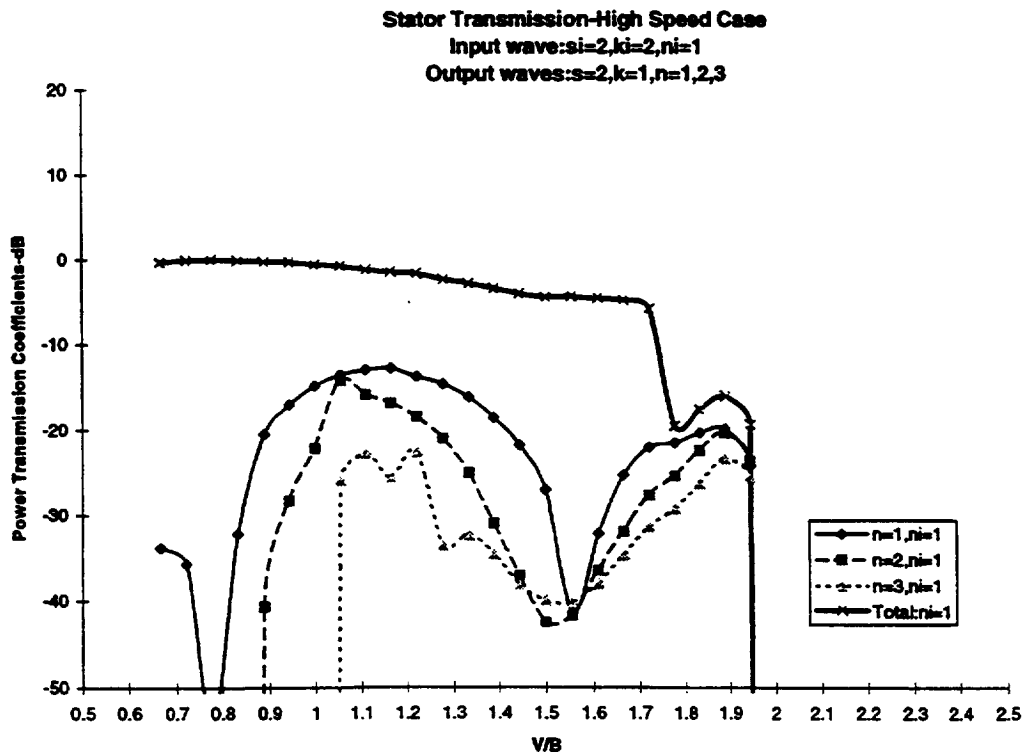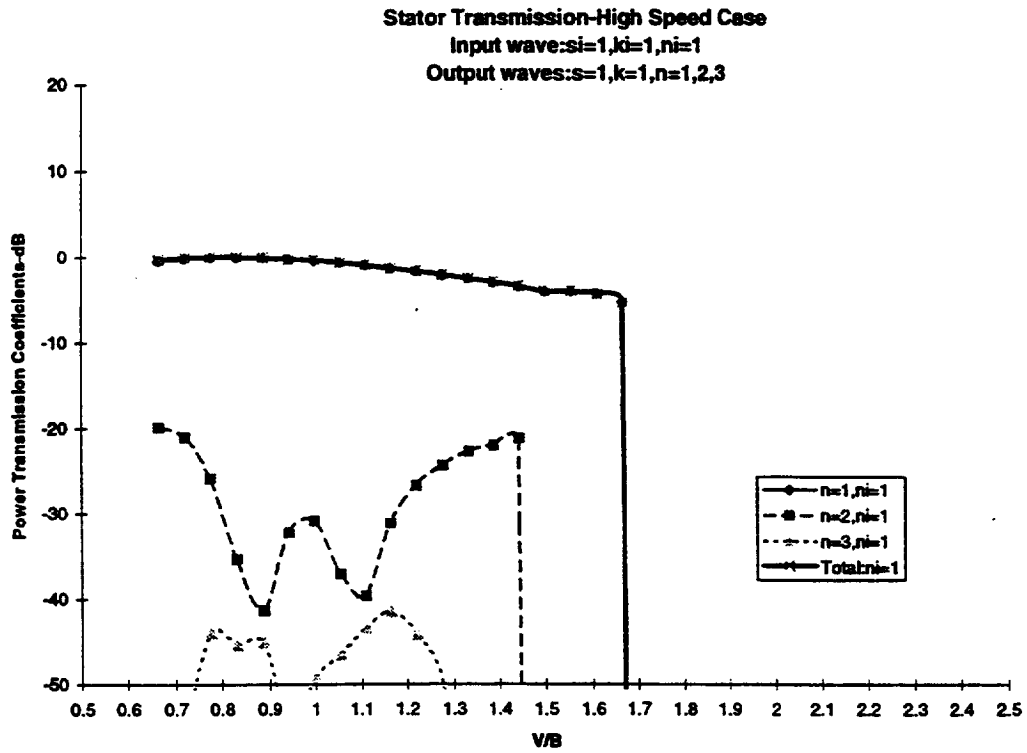
BSI type points, for the stator, occur when input waves are parallel to the vane chords. Because of this orientation, we might expect peaks in the reflection curves and low values in the transmission curves for this case. However, these peaks and low values did not occur for the reflection and transmission BSI points we see at $V/B = 1.45$ in Fig. 3.1, as well as on other curves not shown. In fact, in some of these cases, BSI reflection points were near local minimums. We might also have expected, here, even more than for the other special points, to have seen a special effect, because, unlike in the case for the other special points (see Appendix B), the formula for V/B, Eq. (B.12) does not depend on r. However, no special effect occurred. The same was true for the two-dimensional situation. There can also be BSR points, corresponding to reflected broadside output waves. However, none of the values of points for this condition fell on the curves that were generated. They generally were calculated to be near cut on or cut off, but were located in regions where the curves were cut off. Near these locations, the formulas for BSR and cut-off points were similar, but not identically the same.

For the rotor, special points are shown in Fig. 3.2. Generally, the behavior is consistent with that for the stator case. In particular, for the VBI case, transmission power is high and reflection low, as was the case for the stator. There is a difference, however, for the MO point in the reflection curve of Fig. 3.2. It is not near a dip as it was for the stator case. Also different from the stator case, there is a BSR point that falls on one of the curves (at $V/B = 0.74$).

Note that, when we compare three-dimensional plots with two-dimensional ones, we observe that some of the effects are not as pronounced. For example, in the three-dimensional case, peaks and dips are generally not as sharp. This muted effect, most likely, is a result of the fact that, for three dimensions, the behavior for special points is actually spread over a range of V/B's, rather than being located at just one point. This spread of special points, in turn, occurs because of the radial dependence in many of the formulas in Appendix B.

The scattering curves here and in Ref. 7 were studied at great length to discover whether there were any general trends. Observations resulting from this effort are presented in what follows. Plots for both the mid speed and high speed cases are treated together because they were similar. Regarding reflection for the stator, we saw no real patterns. However, for the most part, we did observe low reflection and high transmission over much of the V/B range. For transmission, waves scattered primarily one mode into itself, but this was not always the case. Examples of where this behavior occurred are the transmission of mode (1,1,1) into (1,1,1) in Figs. 3.1 and Fig. 3.3. When this behavior fails on a portion of the V/B range, mainly because the input wave is cut on but the output one is not, then scattered waves with a lower k and the same or higher n frequently predominate. See, for example, Fig. 3.4 for input wave (2,2,1), with output waves (2,1,1), (2,1,2), and (2,1,3) predominating at higher V/B. Note that below $V/B = 1.7$ on Fig. 3.4, modes not shown are dominating.

Regarding the rotor, it was found, for the two-dimensional situation in Ref. 2, that, for input waves at BPF, reflected energy was primarily into upper harmonics over a wide range of the V/B span. Also, there was sizable transmission loss over the majority of the V/B range on curves not shown. The energy that makes it through is scattered into higher harmonics. Regarding three-dimensional reflection, as for the two-dimensional case, most of the reflected energy, with

Stator Transmission-High Speed Case
Input wave:si=1,ki=1,ni=1
Output waves:s=1,k=1,n=1,2,3

FIGURE 3.3   STATOR TRANSMISSION – FUNDAMENTAL (1,1,1) MODE INPUT

Stator Transmission-High Speed Case
Input wave:si=2,ki=2,ni=1
Output waves:s=2,k=1,n=1,2,3

FIGURE 3.4   STATOR TRANSMISSION – 2xBPF (2,2,1) MODE INPUT

- 20 -

input waves at BPF, appears in upper harmonics, over most of the V/B range. See, for example, Figs. 3.5 - 3.7 for the (1,1,1) input wave. The effect is not as pronounced, if it exists at all, above BPF. Three-dimensional transmission is different from two-dimensional transmission. We did not see substantial transmission loss over most of the V/B range, as was the case for two dimensions. In fact, we observed very little. Additionally, we observed individual modes transmitting primarily into themselves, e.g. (1,1,2) into (1,1,2) in Fig. 3.8, or modes transmitting not only into themselves but into themselves and also into modes with the same (s, k) but with closeby n's, e.g. mode (2,2,2) into (2,2,1), (2,2,2), and (2,2,3) in Fig. 3.9.

Just as in the two-dimensional case, we investigated scattering curves to see whether there was increased reflection at the higher speed. As for the two-dimensional situation, this was not the case. The reason it is not the case, most likely, is because we are looking at individual waves, rather than rays.

Note that, for the rotor, we sometimes had reflection and transmission power ratios greater than one, i.e., dB values greater than zero. Discussion in Ref. 2 shows why this is possible for the two-dimensional case. These ideas carry over analogously to the three-dimensional situation, though this case is a bit more complicated. Physically, what is happening is that the energy in scattered waves is increased by the rotation of the blades.
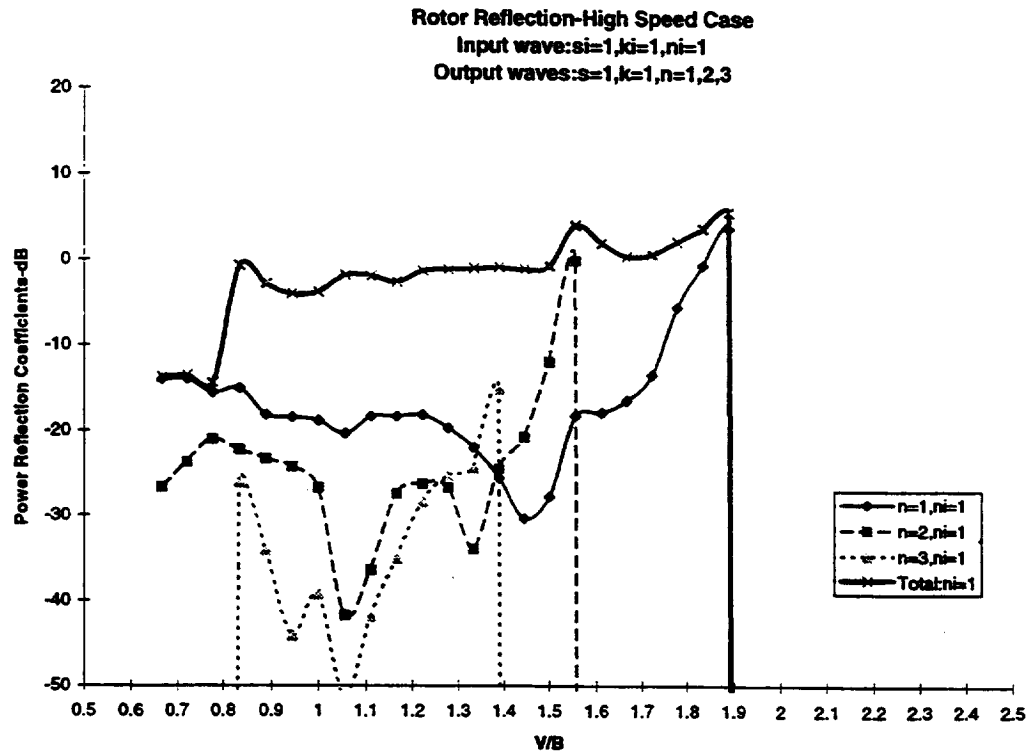
FIGURE 3.5 ROTOR REFLECTION – FUNDAMENTAL (1,1,1) MODE INPUT. OUTPUT AT BPF. "TOTAL" INCLUDES 1, 2, AND 3xBPF AND IS REPEATED IN FIGS. 3.6 AND 3.7
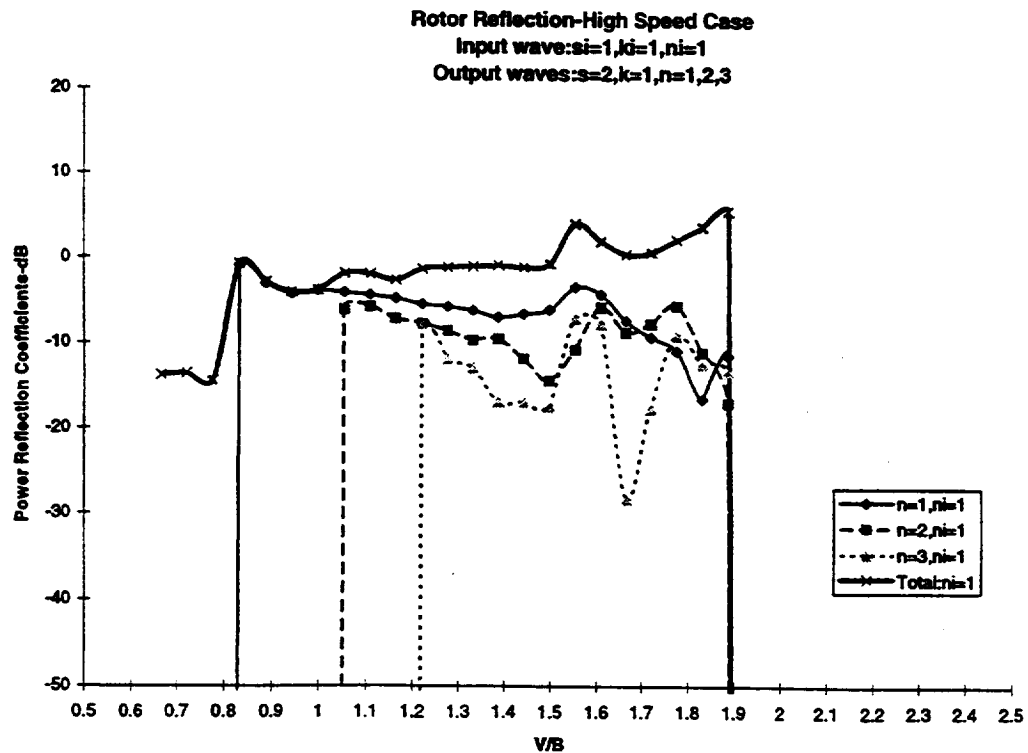

FIGURE 3.6 ROTOR REFLECTION – FUNDAMENTAL (1,1,1) MODE INPUT. OUTPUT AT 2xBPF
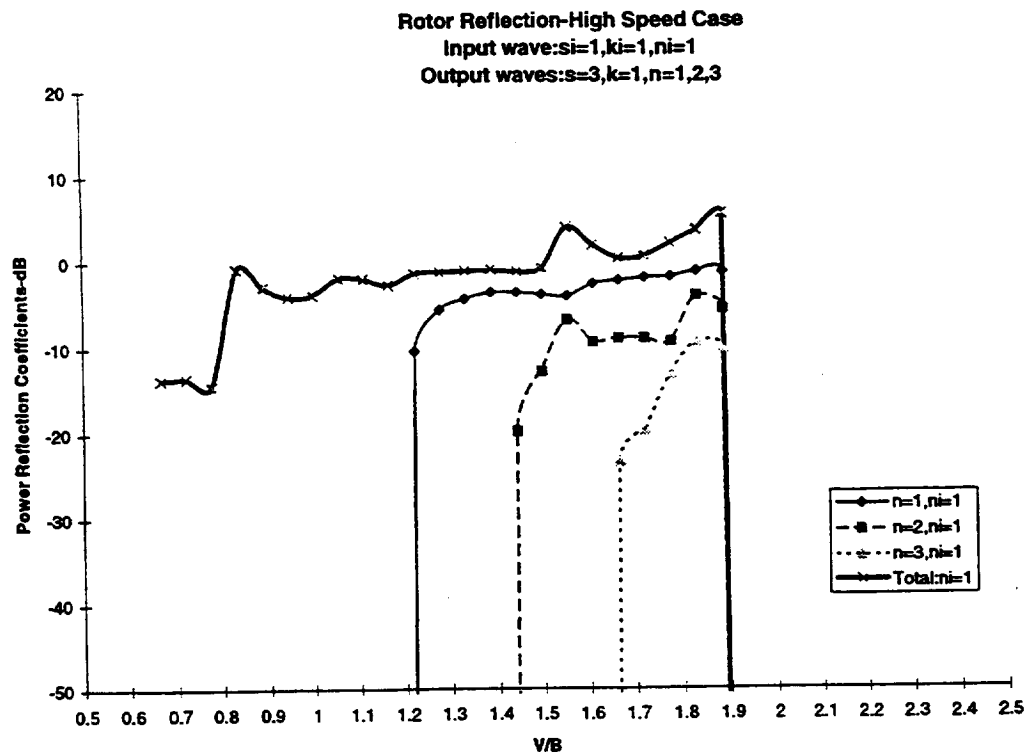
Rotor Reflection-High Speed Case
Input wave:si=1,ki=1,ni=1
Output waves:s=3,k=1,n=1,2,3

Legend:
- n=1,ni=1
- n=2,ni=1
- n=3,ni=1
- Total:ni=1

FIGURE 3.7 ROTOR REFLECTION – FUNDAMENTAL (1,1,1) MODE INPUT. OUTPUT AT 3xBPF

Rotor Transmission-Mid Speed Case
Input wave:si=1,ki=1,ni=2
Output waves:s=1,k=1,n=1,2,3

Legend:
- n=1,ni=2
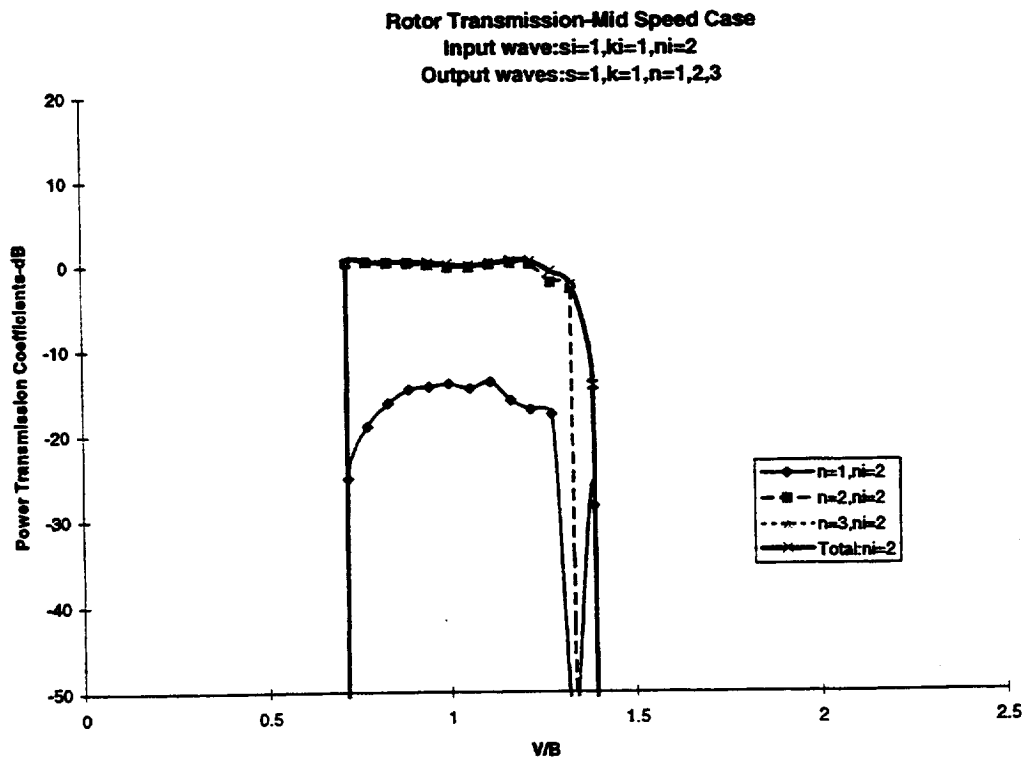- n=2,ni=2
- n=3,ni=2
- Total:ni=2

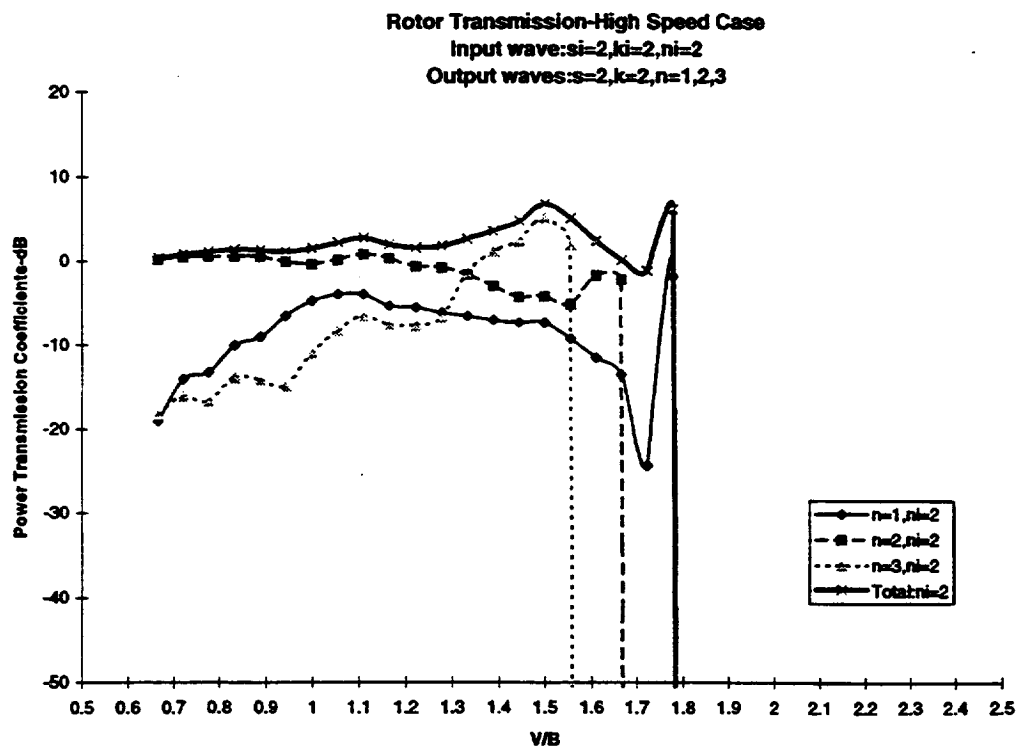**FIGURE 3.8 ROTOR TRANSMISSION – 2ND RADIAL (1,1,2) MODE INPUT**

FIGURE 3.9   ROTOR TRANSMISSION – (2,2,2) MODE INPUT

CHAPTER 4

CONCLUDING REMARKS

This report has employed the three-dimensional SOURCE3D Rotor Wake/Stator Interaction Code to study the scattering coefficients for rotor and stator blade rows. A very large number of reflection and transmission plots have been derived and investigated for trends. These plots are for ratios of output to input wave power versus vane/blade ratio. Power ratios are dB values. Results have been compared to previous two-dimensional results of D. B. Hanson.

To further understand the plots, formulas were derived for predicting special points where there were types of wave alignment or where other conditions existed. It was found that for points where the normal distance between vanes or blades was half the acoustic wavelength, high power levels were produced. This result was in contrast to the two-dimensional situation. This condition is called "load divergence." A second condition, that of "channel resonance," where standing waves could possibly form in the channels between blades or vanes, similar to the two-dimensional case, produced no distinctive results. Another condition, "duct resonance," which sometimes occurs near cut on, was seen to produce unrealistically high power predictions. These values are caused by limitations in the earlier V072 Rotor Wake/Stator Interaction Code, portions of which are used in SOURCE3D. Such values are easily recognized when they occur.

It was discovered that for wave fronts normal to vane or blade chords, the "venetian blind" case, input waves transmit through with virtually no scattering, and transmission power is high. For the stator, when only the output waves are perpendicular to the chords, we have the "modal" case. These waves cannot couple to the loading dipoles, and they generally produce dips in the curves. This pattern, however, was not seen for the rotor case. When input waves are oriented parallel to chords, in the "broadside" case, we might anticipate that there would be high reflection and low transmission. However, this did not happen. These "venetian blind" and "broadside" results were similar to the ones for two dimensions.

Regarding general trends, it was seen for the stator that there was generally high transmission and low reflection over most of the vane/blade ratio range. For transmission, modes generally scattered into themselves, but this was not always the case. For the rotor, we found very little transmission loss, and, in a large number of cases, we found modes transmitting into themselves, or into modes with the same blade and vane harmonic indices and with the same or closeby radial indices. These three-dimensional rotor results were different from their two-dimensional counterparts. We also saw that, for the rotor, scattered energy could be greater than input wave energy by virtue of energy supplied by blade motion.

It is hoped that work in this report will serve to shed light on the complex phenomena of rotor and stator scattering. It is also hoped that this report will assist others in understanding more fully the behavior of the rotor and stator source elements in the TFaNS (the Theoretical Fan Noise Design/Prediction System), of which SOURCE3D is a part.

APPENDIX A

SOUND POWER RELATIONS

In this appendix, we will derive the expression for acoustic power for a standard pressure wave

$$p(x_1, r, \phi, t) = p_{\infty} \sum_{s=-\infty}^{\infty} \sum_{k=-\infty}^{\infty} \sum_{n=1}^{\infty} A_{skn} \Psi_{mn}(r) e^{i(m\phi - \gamma_{skn} x_1 - sB\Omega t)}, \tag{A.1}$$

at an arbitrary axial interface, $x_P = 0$, in an annular duct. Notation is the same as that defined previously in Chapters 1 and 2; and Eq. (A.1) comes from Eq. (2.1), only now the indices P and W are omitted for convenience – they are not needed for the derivation. Once we have the expression for acoustic power, we will use it to obtain the ratio of output to input wave power. The approach here is similar to that in Appendix C of Ref. 5, so the reader is referred there for additional detail when needed. The major difference between the work in Ref. 5 and the work here is that swirl is included in the present derivation (approximately, via a coordinate transformation), whereas it was not included before.

As in to Ref. 7, the acoustic energy flux vector, I, is given by

$$I = \left(\frac{p}{\rho_0} + u \cdot U \right) (\rho_0 u + \rho U), \tag{A.2}$$

where p, ρ, and u are the perturbation pressure, density, and velocity, and ρ_0 and U are the mean flow density and velocity. From this equation, the axial component I_{ax} of I is easily seen to be

$$I_{ax} = \left(\frac{p}{\rho_0} + Uu + Vv \right) (\rho_0 u + U\rho), \tag{A.3}$$

where u, v and U, V are the axial and transverse velocity components of u and U, respectively, which makes V, also, the swirl component. This equation then can be transformed to

$$I_{ax} = \left(1 + M^2 \right) pu* + \frac{M}{\rho_0 c_0} pp* + \rho_0 c_0 M uu*$$
$$- \rho_0 c_0 \frac{\Omega_s r}{c_0} uv* - M \frac{\Omega_s r}{c_0} pv*, \tag{A.4}$$

applying $\rho = p / c_0^2$, $M = U / c_0$, $pu = pu*$, $uu = uu*$, $uv = uv*$, $pv = pv*$, and $V = -\Omega_s r$. Also, Ω_s is swirl flow rotational speed, and $u*$ and $v*$ are the complex conjugates of u and v. The

values of the quantities in Eq. (A.4) are specific to the duct region where a particular wave is located. Thus these values could be different for the input and the output waves involved in a power ratio.

It is shown in Ref. 4 that the axial and transverse velocities associated with p can be written as

$$u(x_1, r, \phi, t) = a_\infty \sum_{s=-\infty}^{\infty} \sum_{k=-\infty}^{\infty} \sum_{n=1}^{\infty} u_{skn} A_{skn} \Psi_{mn}(r) e^{i(m\phi - \gamma_{skn} x_1 - sB\Omega t)}, \tag{A.5}$$

$$v(x_1, r, \phi, t) = a_\infty \sum_{s=-\infty}^{\infty} \sum_{k=-\infty}^{\infty} \sum_{n=1}^{\infty} v_{skn} A_{skn} \Psi_{mn}(r) e^{i(m\phi - \gamma_{skn} x_1 - sB\Omega t)}, \tag{A.6}$$

where

$$u_{skn} = \frac{p_\infty \gamma_{skn}}{a_\infty \rho_0 \lambda_{skn}}, \tag{A.7}$$

$$v_{skn} = \frac{p_\infty m}{a_\infty \rho_0 r \lambda_{skn}}, \tag{A.8}$$

and

$$\lambda_{skn} = -sB\Omega - U\gamma_{skn} + m\Omega_s. \tag{A.9}$$

The parameter a_∞ is the far-field speed of sound and γ_{skn} is the axial wavenumber, given by

$$\gamma_{skn} = \frac{1}{\beta^2} \left[M \left(\frac{sB\Omega - m\Omega_s}{c_0} \right) \pm k_{skn} \right], \tag{A.10}$$

where

$$k_{skn} = \sqrt{\left(\frac{sB\Omega - m\Omega_s}{c_0} \right)^2 - \beta^2 \kappa_{mn}^2} \tag{A.11}$$

and

$$\beta = \sqrt{1 - M^2}. \tag{A.12}$$

The sound power flux through a cross-section of the duct, which will give the power we seek, is given (see Ref. 7) by

$$Power = \int_{A_D} <I_{ax}> dA, \tag{A.13}$$

where $<I_{ax}>$ is the acoustic intensity,

$$< I_{ax} > = \frac{B\Omega}{2\pi} \int_{-\pi/B\Omega}^{\pi/B\Omega} I_{ax} dt , \qquad (A.14)$$

and A_D is the duct cross-sectional area. Then, using Eqs. (A.1), (A.4)-(A.6), and (A.14), while proceeding the same as in Ref. 5, Eq. (A.13) can be evaluated to give that

$$Power = \frac{\pi(r_D^2 - r_H^2)p_\infty^2}{\rho_0 U} \sum_{k=-\infty}^{\infty} \sum_{n=1}^{\infty} \sum_{s=-\infty}^{\infty} [\tilde{G}_{skn} + \hat{G}_{skn}]|A_{skn}|^2 , \qquad (A.15)$$

where

$$\tilde{G}_{skn} = M^2 - (1 + M^2)C_{skn}^* + |C_{skn}|^2 , \qquad (A.16)$$

$$\hat{G}_{skn} = -\frac{\Omega_s}{Mc_0} C_{skn} D_{skn}^* + \frac{M\Omega_s}{c_0} D_{skn}^* , \qquad (A.17)$$

and

$$C_{skn} = \frac{\gamma_{skn}}{\left(\frac{sB\Omega - m\Omega_s}{U}\right) + \gamma_{skn}} , \qquad (A.18)$$

$$D_{skn} = \frac{m}{\left(\frac{sB\Omega - m\Omega_s}{U}\right) + \gamma_{skn}} . \qquad (A.19)$$

We can simplify $\tilde{G}_{skn}$ and $\hat{G}_{skn}$ to give

$$\tilde{G}_{skn} = \frac{\mp M^2\beta^4 \left(\frac{sB\Omega - m\Omega_s}{U}\right)k_{skn}}{\left[\left(\frac{sB\Omega - m\Omega_s}{c_0}\right) \pm Mk_{skn}\right]^2} , \qquad (A.20)$$

$$\hat{G}_{skn} = \frac{\mp mM^2 \left(\frac{\Omega_s}{U}\right)\beta^4 k_{skn}}{\left[\left(\frac{sB\Omega - m\Omega_s}{c_0}\right) \pm Mk_{skn}\right]^2} , \qquad (A.21)$$

where the upper set of signs in each equation corresponds to upstream-going waves and the lower ones to downstream-going waves. From these relations, we can deduce that

$$G_{skn} = \tilde{G}_{skn} + \hat{G}_{skn}$$

$$= \frac{\mp M^2 \beta^4 \left(\frac{sB\Omega}{U}\right) k_{skn}}{\left[\left(\frac{sB\Omega - m\Omega_s}{c_0}\right) \pm M k_{skn}\right]^2}. \tag{A.22}$$

Thus Eq. (A.15) can be written, finally, as

$$Power = \frac{\pi(r_D^2 - r_H^2)p_\infty^2}{\rho_0 U} \sum_{k=-\infty}^{\infty} \sum_{n=1}^{\infty} \sum_{s=-\infty}^{\infty} G_{skn} |A_{skn}|^2. \tag{A.23}$$

Because we are dealing with scattering coefficients, we are interested in power ratios, $\Re$, rather than just straight power. Using individual terms from Eq. (A.23) for the power of input mode (si, ki, ni) and of output mode (s, k, n), we have*

$$\Re = \frac{Power_{out}}{Power_{in}} = \frac{\rho_{0,out}U_{out}}{\rho_{0,in}U_{in}} \frac{G_{skn}}{G_{s_ik_in_i}} |S_{skn;s_ik_in_i}|^2, \tag{A.24}$$

where the subscripts "in" and "out" refer to input and output waves. Also, we have used that the scattering coefficient, $S_{skn;s_ik_in_i}$, is given by $A_{skn}/A_{s_ik_in_i}$.

Finally, using Eq. (A.22) for G_{skn} and $G_{s_ik_in_i}$; applying the relation $c_0^2 = \gamma p_0/\rho_0$, where γ is the specific heat ratio for air and p_0 is the mean flow pressure; letting M_T be the rotor blade tip rotational Mach number and M_s the swirl rotational Mach number at the rotor tip; then Eq. (A.24) can be written as

$$\Re = \frac{c_{0,in}/p_{0,in}}{c_{0,out}/p_{0,out}} \left(\frac{\beta_{out}}{\beta_{in}}\right)^4 \left[\frac{sBM_{T,out} - m_{out}M_{s,out} \pm M_{out}\tilde{k}_{skn,out}}{s_iBM_{T,in} - m_{in}M_{s,in} \pm M_{in}\tilde{k}_{s_ik_in_i,in}}\right]^2$$

$$\times \frac{sM_{T,out}}{s_iM_{T,in}} \frac{\tilde{k}_{skn}}{\tilde{k}_{s_ik_in_i}} |S_{skn;s_ik_in_i}|^2, \tag{A.25}$$

---

* Note that when coding the power ratio for use with SOURCE3D, Eq. (A.24), must be multiplied by a term $|\psi_{max,in}/\psi_{max,out}|$, where $\psi_{max,in}$ and $\psi_{max,out}$ are the maximum values, radially, of the input and output radial mode functions involved. This is to compensate for the fact that the radial mode functions actually used in the code are not normalized to +1. In the definition of the scattering coefficients $S_{skn;s_ik_in_i}$, they are assumed normalized to +1.

where $\widetilde{k}_{skn} = k_{skn} r_D$. For the plots, we use decibel values. Thus what is actually used is

$$\mathfrak{R}_{dB} = 10 \log_{10} \mathfrak{R}.$$

(A.26)

APPENDIX B

SPECIAL VANE/BLADE RATIOS

This section develops the relationships presented in Section 2.2 that are used to locate special behavior on the scattering curves. The locations are given in terms of vane/blade (V/B), or blade/vane (B/V), ratio. At times, detail here will be brief; when this is the case, the reader might wish to refer to Ref. 2, where the two-dimensional case is treated and details are similar.

Cut-On Range. Corresponding to the discussion in the main body of the report, the first set of points is actually a range of points. Cut on is discussed thoroughly in Refs. 2 and 5, and elsewhere. For the three-dimensional case, it occurs when the square root in the expression for γ^P_{Wskn}, Eq. (2.2), i.e. the k^P_{Wskn} part, given by Eq. (2.3), is real. Then γ^P_{Wskn} is real, and the wave propagates with no attenuation in the axial direction. When the square root becomes zero, we are at the *cut-off point*. As the expression inside the square root becomes negative, the square root becomes imaginary and the $e^{i\gamma^P_{Wskn}}$ factor in the expression for a wave, Eq. (2.1), decays.

Proceeding much as for the two-dimensional case (Ref. 2), we can set the square root in Eq. (2.3) equal to zero and solve for M_T at cut off. We obtain

$$M_T = M_s \pm \beta\left(\frac{\kappa_{mn}}{m}\right) - \left[M_s \pm \beta\left(\frac{\kappa_{mn}}{m}\right)\right]\left(\frac{kV}{sB}\right)_{cutoff}. \qquad (B.1)$$

Similar to the two-dimensional case, Eq. (B.1) allows us to draw a sketch showing the cut-on range for V/B for each value of M_T for a fixed radial index n. The sketch is shown in Fig. 2.2. The dependence on n comes from κ_{mn} in Eq. (B.1). The values of m change as V/B changes. Note that for the two-dimensional case, $(\kappa_{mn}/m) \to 1$, so the boundaries in Fig. 2.2 for such a case would be straight lines. For three dimensions, κ_{mn}/m will vary as V/B changes, so the two lines bounding the cut-on range will not necessarily be straight. However, the variation is so small, that generally, for all intents and purposes, the lines are straight, and that is the way they have been drawn in Fig. 2.2. At any rate, please note that there is a range of V/B values for which waves are cut on. Also note that, in Fig. 2.2, there are regions indicated where m is either positive or negative; how these regions are determined is discussed in Ref. 2.

Half Wavelength (Load Divergence) Points. Half wavelength points occur when the normal distance between vanes or blades is the same as half the sound wavelength in free space. For the stator (refer to Fig. B.1), the distance between vanes, at each radius, is $(2\pi r / V)\cos\alpha_s$, and the free space wavelength λ is $(2\pi c / sB\Omega)$, since the frequency is $(sB\Omega / 2\pi)$, where c is the free space speed of sound. Hence,
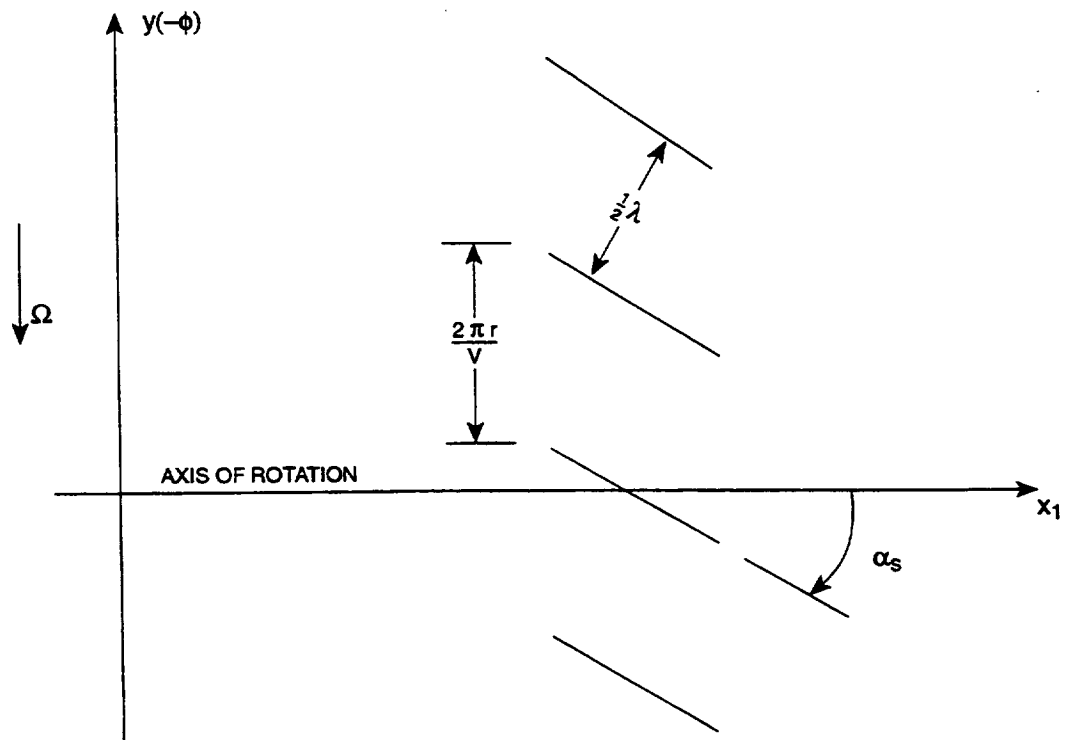
FIGURE B.1 STATOR CASCADE (INTERSECTION OF STATOR VANES WITH CYLINDRICAL SURFACE OF RADIUS r)

$$\frac{2\pi r}{V}\cos\alpha_S = \frac{\pi c}{sB\Omega},$$
(B.2)

and

$$\frac{V}{sB} = 2\left(\frac{\Omega r}{c}\right)\cos\alpha_S,$$
(B.3)

$$= 2M_T\left(\frac{r}{r_D}\right)\cos\alpha_S, \qquad \frac{r_H}{r_D} \le \frac{r}{r_D} \le 1.$$

Note that V/B depends on the radial location r. In analyzing run output data, we have observed that blade loading is very high when there is load divergence and this high value is only needed at one or more radial stations in $r_H \le r \le r_D$ to cause load divergence. Generally, when there is load divergence, the high loading occurs near $r = r_H$. Applying this information, Eq. (B.3) then gives the vane/blade ratio for load divergence,

$$\frac{V}{sB} = 2M_T\left(\frac{r_H}{r_D}\right)\cos\alpha_{S,H},$$
(B.4)

where $\alpha_{S,H}$ is the stator stagger angle at the hub. Similarly, for the rotor, we have load divergence at

$$\frac{B}{kV} = 2M_T\left(\frac{r_H}{r_D}\right)\cos\alpha_{R,H},$$
(B.5)

where $\alpha_{R,H}$ is the negative of the rotor stagger angle at the hub. Eq. (B.4) was used to identify the load divergence points (labeled ½WP) in Fig.3.1.

Channel Resonance Points. Channel resonance occurs when the distance between nodes of a standing wave located between two adjacent vanes or blades is the same as the length of the channel (i.e., the chord). The same formula that was derived for the stator in Ref. 2 for the two-dimensional case also holds for the three-dimensional case. Thus we have

$$\frac{V}{sB} = \frac{\Omega r / c}{(1 - M_{rS}^2)\left(\frac{q}{2}\right)\left[\frac{2\pi r}{V(2b)}\right]}.$$
(B.6)

However, now r is not one fixed value, but varies over vane span. The same is true for b, the vane semi-chord. In Eq. (B.6), M_{rS} is the relative Mach number for the stator vane rows and q is any non-zero integer.

This equation can be rewritten as

$$\frac{V}{sB} = \frac{\left(\dfrac{\Omega r_D}{c}\right)\left[\dfrac{V(2b)}{2\pi r_D}\right]}{(1-M_{rS}^2)\left(\dfrac{q}{2}\right)} = \frac{M_T \sigma_S \left(\dfrac{b}{b_T}\right)}{(1-M_{rS}^2)\left(\dfrac{q}{2}\right)},$$ (B.7)

where $\sigma_S = \dfrac{V(2b)}{2\pi r_D}$ is the solidity of the stator, and b_T is the semi-chord at the vane tip. To find the particular value of V/B where the channel resonance effect might be the greatest, we set $r/r_D = 0.8$, roughly where maximum loading occurs for cases other than load divergence. Thus in Eq. (B.7) it is to be assumed that σ_S and b/b_T are evaluated at $r/r_D = 0.8$. Similarly, for the rotor, we have

$$\frac{B}{kV} = \frac{M_T \sigma_R \left(\dfrac{b_R}{b_{RT}}\right)}{(1-M_{rR}^2)\left(\dfrac{q}{2}\right)},$$ (B.8)

where $\sigma_R = \dfrac{B(2b_R)}{2\pi r_D}$ is the solidity of the rotor, b_R is the blade semi-chord, b_{RT} is the semi-chord at the blade tip, and M_{rR} is the relative Mach number for the rotor blade rows. As for the stator, quantities on the right-hand side of Eq. (B.8) are evaluated at $r/r_D = 0.8$. Note that, in computer runs, σ_S and σ_R were kept constant. Also, for the particular geometry studied, b/b_T was constant; however, b_R/b_{RT} was not. Eqs. (B.7) and (B.8) were used to identify the channel resonance points (labeled CR) in Figs. 3.1 and 3.2.

Broadside, Venetian Blind, and Modal Points. Broadside, venetian blind, and modal points are defined in Section 2.2. They are points where wavefronts are either parallel or perpendicular to stator vanes or rotor blades. To find the V/B values where these conditions occur, we first derive formulas in terms of arbitrary wavefront slopes, then substitute in values for the particular cases. Consider the exponential term $e^{i(m\phi - \gamma_{skn}x_1 - sB\Omega t)}$ in Eq. (2.1) for a standard wave, where x^P has been taken to be zero and where, for convenience, P and W are omitted. Because a wavefront is a line having constant phase at any given time, this term tells us that these lines are the the ones where $m\phi - \gamma_{skn}x_1 = constant$. Using the coordinates in Fig. B.1 and converting from polar to Cartesian coordinates, we have that $\phi = -y/r$. Hence, wavefronts are defined by the relation

$$\frac{m}{r}y = -\gamma_{skn}x_1 + constant,$$ (B.9)

at any fixed value of radius r.

The slope of this line is $-\gamma_{skn}r/m$. Therefore, recalling Eq. (2.2), the slope $\mathcal{b}$ of the wavefront can be written as

$$b = -\frac{1}{\beta^2}\left(\frac{r}{r_D}\right)\left[M\left(\frac{sBM_T}{m} - M_s\right) \pm \text{sgn}(m)\sqrt{\left(\frac{sBM_T}{m} - M_s\right)^2 - \beta^2\left(\frac{\kappa_{mn}}{m}\right)^2} \right]. \tag{B.10}$$

In Eq. (B.10) and throughout the rest of this section, the upper and lower signs refer, respectively, to upstream- and downstream-going waves. For the stator case, Eq. (B.10) can be solved for (kV/sB) to give

$$\frac{kV}{sB} = 1 - \frac{M_T}{M_s + Mb\left(\frac{r_D}{r}\right) \pm \sqrt{\left(\frac{\kappa_{mn}}{m}\right)^2 + b^2\left(\frac{r_D}{r}\right)^2}}. \tag{B.11}$$

For the broadside case, it can be seen from the Mach-number triangle in Fig. 2.3 that $b = -\left(\frac{M_s}{M}\right)\left(\frac{r}{r_D}\right)$. Substituting this relation in Eq. (B.11), then

$$\frac{kV}{sB} = 1 \mp \frac{M_T}{\sqrt{\left(\frac{\kappa_{mn}}{m}\right)^2 + \left(\frac{M_s}{M}\right)^2}}. \tag{B.12}$$

Upper and lower signs in Eq. (B.12) have been set based on physical arguments discussed in Ref. 2. This will also be the case for analogous formulas later in this section. Note that (kV/sB) in Eq. (B.12) does not depend on r. This means that waves are "broadside" at all radii for the V/B ratio of Eq. (B.12). Thus, we might expect large reflection at this vane/blade ratio. However, in practice this does not turn out to be the case. Also note that Eq. (B.12) does not give V/B explicitly, because κ_{mn}/m on the right depends on V/B. Therefore, to find V/B from Eq. (B.12), we must iteratively determine values of κ_{mn}/m for different values of V/B, from computer run data, until the equation is satisfied.

From the Mach-number triangle in Fig. 2.5, we see that the wavefront slope for the venetian blind case is $b = \left(\frac{M}{M_s}\right)\left(\frac{r_D}{r}\right)$. The same is true for the modal case. Hence for these cases,

$$\frac{kV}{sB} = 1 - \frac{M_T}{M_s + \left(\frac{M^2}{M_s}\right)\left(\frac{r_D}{r}\right)^2 \mp \sqrt{\left(\frac{\kappa_{mn}}{m}\right)^2 + \left(\frac{M}{M_s}\right)^2\left(\frac{r_D}{r}\right)^4}}. \tag{B.13}$$

To eliminate radial dependence, we set $r/r_D = 0.8$. Because peak loads occur near this location, we would expect that this value would give a vane/blade ratio providing maximum effect. We have

-35-

$$\frac{kV}{sB} = 1 - \frac{M_T}{M_s + 1.5625\left(\frac{M^2}{M_s}\right) \mp \sqrt{\left(\frac{\kappa_{mn}}{m}\right)^2 + 2.4414\left(\frac{M}{M_s}\right)^2}}. \tag{B.14}$$

For the rotor, we invert both sides of Eq. (B.11) and rewrite it in the form

$$\frac{sB}{kV} = 1 - \frac{M_T}{M_T - M_s - Mb\left(\frac{r_D}{r}\right) \pm \sqrt{\left(\frac{\kappa_{mn}}{m}\right)^2 + b^2\left(\frac{r_D}{r}\right)^2}}. \tag{B.15}$$

Then for the broadside case, we see from the Mach-number triangle in Fig. 2.4 that the slope b is given by $b = \frac{M_s - M_T}{M}\left(\frac{r}{r_D}\right)$. Thus Eq. (B.15) gives the formula

$$\frac{sB}{kV} = 1 \mp \frac{M_T}{\sqrt{\left(\frac{\kappa_{mn}}{m}\right)^2 + \left(\frac{M_s - M_T}{M}\right)^2}}. \tag{B.16}$$

As for the stator broadside case, Eq. (B.12), this relation also does not depend on r. For the venetian blind and modal rotor cases, b is the negative of the reciprocal of that for the broadside case, i.e., $b = \frac{M}{M_T - M_s}\left(\frac{r_D}{r}\right)$. Using this in Eq. (B.15) and taking $r_D/r = 0.8$, we then have

$$\frac{sB}{kV} = 1 - \frac{M_T}{M_T - M_s - 1.5625\left(\frac{M^2}{M_T - M_s}\right) \mp \sqrt{\left(\frac{\kappa_{mn}}{m}\right)^2 + 2.4414\left(\frac{M}{M_T - M_s}\right)^2}}. \tag{B.17}$$

Eqs. (B.12) and (B.16) were used to identify the broadside points (labeled BSI and BSR) in Figs. 3.1 and 3.2. Eqs. (B.14) and (B.17) were used to identify the venetian blind and modal points (labeled VBI and MO) in Figs. 3.1 and 3.2.

REFERENCES

1. Topol, D. A., "TFaNS Theoretical Fan Noise Design/Prediction System, Volume 1: System Description, CUP3D Technical Documentation and Manual for Code Developers," NASA CR, 1997.

2. Hanson, D. B., "Acoustic Reflection and Transmission of 2-Dimensional Rotors and Stators, Including Mode and Frequency Scattering Effects," NASA CR, 1997.

3. Hanson, D. B., "Mode Trapping in Coupled 2D Cascades – Acoustic and Aerodynamic Results," AIAA Paper 93-4417, October 1993.

4. Meyer, H. D., "Source Methodology for Turbofan Noise Prediction (SOURCE3D Technical Documentation)," NASA CR, 1997.

5. Meyer, H. D. and E. Envia, "Acoustic Analysis of Turbofan Noise Generation," NASA CR-4715, March 1996.

6. Smith, S. N., "Discrete Frequency Sound Generation in Axial Flow Turbomachines," Aeronautical Research Council Reports and Memoranda, No. 3709, March 1972.

7. Meyer, H. D., "Acoustic Scattering by Three-Dimensional Stators and Rotors Using the SOURCE3D Code, Volume 2: Scattering Plots," NASA CR, 1997.

8. Goldstein, M. E., *Aeroacoustics*, McGraw-Hill, New York, 1976.

ACKNOWLEDGMENTS

REPORT DOCUMENTATION PAGE

Public reporting burden for this collection of information is estimated to average 1 hour per response, including the time for reviewing instructions, searching existing data sources, gathering and maintaining the data needed, and completing and reviewing the collection of information. Send comments regarding this burden estimate or any other aspect of this collection of information, including suggestions for reducing this burden, to Washington Headquarters Services, Directorate for Information Operations and Reports, 1215 Jefferson Davis Highway, Suite 1204, Arlington, VA 22202-4302, and to the Office of Management and Budget, Paperwork Reduction Project (0704-0188), Washington, DC 20503.

1. AGENCY USE ONLY (Leave blank)	2. REPORT DATE	3. REPORT TYPE AND DATES COVERED
	March 1999	Final Contractor Report

4. TITLE AND SUBTITLE

Acoustic Scattering by Three-Dimensional Stators and Rotors Using the SOURCE3D Code

Volume 1: Analysis and Results

5. FUNDING NUMBERS

WU–538–03–11–00

NAS3–26618

6. AUTHOR(S)

Harold D. Meyer

7. PERFORMING ORGANIZATION NAME(S) AND ADDRESS(ES)

United Technologies Corporation
Hamilton Standard Division
1 Hamilton Road
Windsor Locks, Connecticut 06096

8. PERFORMING ORGANIZATION REPORT NUMBER

E–11619

9. SPONSORING/MONITORING AGENCY NAME(S) AND ADDRESS(ES)

National Aeronautics and Space Administration
John H. Glenn Research Center at Lewis Field
Cleveland, Ohio 44135–3191

10. SPONSORING/MONITORING AGENCY REPORT NUMBER

NASA CR—1999-208885
PWA 6420–105

11. SUPPLEMENTARY NOTES

Project Manager, Dennis L. Huff, NASA Lewis Research Center, organization code 5940, (216) 433–3913.

12a. DISTRIBUTION/AVAILABILITY STATEMENT

Unclassified - Unlimited
Subject Category: 71   Distribution: Nonstandard

This publication is available from the NASA Center for AeroSpace Information, (301) 621–0390.

12b. DISTRIBUTION CODE

13. ABSTRACT (Maximum 200 words)

This report provides a study of rotor and stator scattering using the SOURCE3D Rotor Wake/Stator Interaction Code. SOURCE3D is a quasi-three-dimensional computer program that uses three-dimensional acoustics and two-dimensional cascade load response theory to calculate rotor and stator modal reflection and transmission (scattering) coefficients. SOURCE3D is at the core of the TFaNS (Theoretical Fan Noise Design/Prediction System), developed for NASA, which provides complete fully coupled (inlet, rotor, stator, exit) noise solutions for turbofan engines. The reason for studying scattering is that we must first understand the behavior of the individual scattering coefficients provided by SOURCE3D, before eventually understanding the more complicated predictions from TFaNS. To study scattering, we have derived a large number of scattering curves for vane and blade rows. The curves are plots of output wave power divided by input wave power (in dB units) versus vane/blade ratio. Some of these plots are shown in this report. All of the plots are provided in a separate volume. To assist in understanding the plots, formulas have been derived for special vane/blade ratios for which wavefronts are either parallel or normal to rotor or stator chords. From the plots, we have found that, for the most part, there was strong transmission and weak reflection over most of the vane/blade ratio range for the stator. For the rotor, there was little transmission loss.

14. SUBJECT TERMS

Acoustics; Turbomachinery; Noise; Fans

15. NUMBER OF PAGES

46

16. PRICE CODE

A03

17. SECURITY CLASSIFICATION OF REPORT	18. SECURITY CLASSIFICATION OF THIS PAGE	19. SECURITY CLASSIFICATION OF ABSTRACT	20. LIMITATION OF ABSTRACT
Unclassified	Unclassified	Unclassified	